Article

Neuron

ER Lipid Defects in Neuropeptidergic Neurons Impair Sleep Patterns in Parkinson's Disease

Graphical Abstract

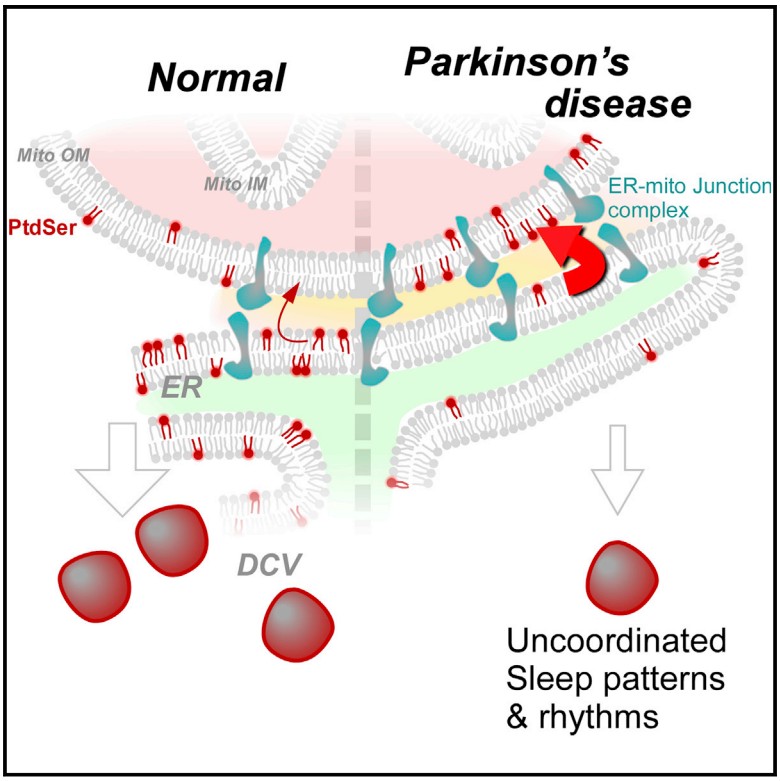

Authors

Jorge S. Valadas, Giovanni Esposito, Dirk Vandekerkhove, ..., Philip Seibler, Christine Klein, Patrik Verstreken

Correspondence

patrik.verstreken@kuleuven.vib.be

In Brief

Valadas et al. show that ER lipid imbalance causes sleep pattern defects in Parkinson's disease by preventing the formation of secretory vesicles required for the release of the neuropeptides. Restoring the ER lipid balance by supplementation with phosphatidylserine rescues the cellular and behavioral defects.

Highlights

- Parkinson's disease (PD) models (*parkin*/*pink1* loss) have circadian and sleep defects
- Increased ER-mitochondria contacts cause neuropeptide accumulation in ER in PD models
- Depletion of phosphatidylserine from ER causes sleep pattern phenotypes in PD models
- Phosphatidylserine supplementation rescues circadian and sleep defects of PD models

Valadas et al., 2018, Neuron *98*, 1–15
June 27, 2018
https://doi.org/10.1016/j.neuron.2018.05.022

CellPress

Please cite this article in press as: Valadas et al., ER Lipid Defects in Neuropeptidergic Neurons Impair Sleep Patterns in Parkinson's Disease, Neuron (2018), https://doi.org/10.1016/j.neuron.2018.05.022

Neuron
Article

CellPress

ER Lipid Defects in Neuropeptidergic Neurons Impair Sleep Patterns in Parkinson's Disease

Jorge S. Valadas,[1,2] Giovanni Esposito,[1,2] Dirk Vandekerkhove,[1,2] Katarzyna Miskiewicz,[1,2,4] Liesbeth Deaulmerie,[1,2] Susanna Raitano,[1,2] Philip Seibler,[3] Christine Klein,[3] and Patrik Verstreken[1,2,5,*]
[1]VIB-KU Leuven Center for Brain and Disease Research, 3000 Leuven, Belgium
[2]Department of Neurosciences, Leuven Brain Institute, KU Leuven, 3000 Leuven, Belgium
[3]Institute of Neurogenetics, University of Lübeck, 23562 Lübeck, Germany
[4]Present address: Universität Osnabrück, 49076 Osnabrück, Germany
[5]Lead Contact
*Correspondence: patrik.verstreken@kuleuven.vib.be
https://doi.org/10.1016/j.neuron.2018.05.022

SUMMARY

Parkinson's disease patients report disturbed sleep patterns long before motor dysfunction. Here, in *parkin* and *pink1* models, we identify circadian rhythm and sleep pattern defects and map these to specific neuropeptidergic neurons in fly models and in hypothalamic neurons differentiated from patient induced pluripotent stem cells (iPSCs). Parkin and Pink1 control the clearance of mitochondria by protein ubiquitination. Although we do not observe major defects in mitochondria of mutant neuropeptidergic neurons, we do find an excess of endoplasmic reticulum-mitochondrial contacts. These excessive contact sites cause abnormal lipid trafficking that depletes phosphatidylserine from the endoplasmic reticulum (ER) and disrupts the production of neuropeptide-containing vesicles. Feeding mutant animals phosphatidylserine rescues neuropeptidergic vesicle production and acutely restores normal sleep patterns in mutant animals. Hence, sleep patterns and circadian disturbances in Parkinson's disease models are explained by excessive ER-mitochondrial contacts, and blocking their formation or increasing phosphatidylserine levels rescues the defects *in vivo*.

INTRODUCTION

Parkinson's disease (PD) affects about 1% of the population older than 60 years (de Lau and Breteler, 2006). Whereas motor symptoms and loss of dopaminergic neurons are hallmarks of the disease (Braak et al., 2003), 99% of the patients report non-motor symptoms that include sleep defects, cognitive impairment, depression, olfactory loss, and constipation (Munhoz et al., 2015). Many patients also suffer from type 2 diabetes mellitus (De Pablo-Fernández et al., 2017). Sleep pattern disturbances are particularly burdensome to Parkinson's disease patients (Politis et al., 2010) and manifest as insomnia, sleep fragmentation, rapid eye movement (REM) sleep behavior disorders, and loss of circadian rhythms (De Cock et al., 2008). These highly prevalent symptoms occur very early in the disease, often years prior to dopaminergic neuron loss and motor symptoms (Lee and Koh, 2015). Furthermore, dopaminergic replacement therapy in Parkinson's disease patients is able to significantly restore motor function but is insufficient to rescue the non-motor symptoms of the disease, including sleep pattern disturbances (Lee and Koh, 2015). This suggests that sleep defects originate from dysfunction of a distinct circuitry. However, the origin of sleep defects in Parkinson's disease remains elusive.

Although Parkinson's disease animal models have been tested for sleep coordination defects, the characteristic defects in circadian rhythmicity, disruption of REM sleep and sleep fragmentation seen in patients, are rarely observed in animal models (Fifel et al., 2016). This is probably because many Parkinson's disease models selectively target the dopaminergic system. Although mice treated with 1-methyl-4-phenyl-1,2,3,6-tetrahydropyridine (MPTP), rotenone, 6-hydroxydopamine (6OHDA), or deficient for vesicular monoamine transported (VMAT) show typical dopaminergic neuron degeneration (Fifel et al., 2016), they do not present the diverse and frequent non-motor symptoms of the disease. In addition, animal models of familial Parkinson's disease, where specific genes are knocked out or pathogenic mutations are expressed, do not present the sleep phenotypes typical of the disease (Fifel et al., 2016). Hence, models that broadly affect the nervous system are needed to study non-motor symptoms of Parkinson's disease.

Whereas Parkinson's disease is primarily a sporadic disease, about 10% is familial (Lill and Klein, 2015). Interestingly, both sporadic and familial Parkinson's disease patients display early-onset sleep defects, suggesting this is fundamental to the disease (De Cock et al., 2008; Kasten et al., 2010). Among Parkinson's disease genes, *parkin* and *pink1* are relatively well studied, and their protein products act in a common pathway to ubiquitinate mitochondrial target proteins, resulting in mitochondrial degradation (Dawson and Dawson, 2010; Valadas et al., 2015). *parkin* encodes for the E3 ubiquitin ligase that catalyzes the ubiquitination of specific targets, guiding them to degradation or to a different cellular location (Pickrell and Youle, 2015). If Parkin function is impaired, its targets accumulate in the cell. Pink1 is a kinase that activates Parkin by phosphorylation (Pickrell and Youle, 2015). Upon mitochondrial depolarization,

Pink1 is stabilized on the outer mitochondrial membrane and recruits Parkin to promote the removal of damaged mitochondria (Pickrell and Youle, 2015). An expected long-term consequence of Parkin or Pink1 loss is the accumulation of dysfunctional mitochondria (Pickrell and Youle, 2015); however, this is not observed in all neuronal cell types *in vivo*. In addition to causative mutations in the *parkin* gene, Parkin protein is also often inactivated in sporadic Parkinson's disease (Dawson and Dawson, 2010), and similar to sporadic Parkinson's disease, patients with *parkin* or *pink1* mutations exhibit sleep pattern defects (Kasten et al., 2010).

Parkin and Pink1 are broadly expressed in the brain (Stichel et al., 2000; Taymans et al., 2006), and in this work, we use loss-of-function mutations in *parkin* and *pink1* and study them both in hypothalamic neurons differentiated from patient induced pluripotent stem cells (iPSCs) and in fruit flies to dissect the molecular, cellular, and neurobiological origin of the circadian and sleep pattern defects in Parkinson's disease. We find that excess transfer of phosphatidylserine at the endoplasmic reticulum (ER)-mitochondrial contacts of mutant neuropeptidergic neurons causes a defect to produce loaded secretory vesicles that control circadian rhythms. Increasing phosphatidylserine levels is sufficient to rescue secretory vesicle production and sleep pattern defects in the Parkinson's disease models.

RESULTS

Parkinson's Disease Models Have Sleep Pattern Defects

The mechanisms of sleep maintenance and circadian rhythmicity control are well conserved across species, including *Drosophila melanogaster* (Hendricks and Sehgal, 2004; Hendricks et al., 2000). Besides a higher threshold to arousal, sleeping flies do not move, and inactivity over a 5-min period is regarded as a good measure of sleep, also verified by alternative methodologies (Chiu et al., 2010; Hendricks et al., 2000). To assess features of circadian rhythmicity, we used automated monitoring to continuously follow the movement of flies that lack *parkin* or *pink1* (Park et al., 2006; Pesah et al., 2004). Interestingly, several aspects of the circadian pattern are disrupted in both *parkin* and *pink1* mutants compared to controls as summarized in Figures 1A and S1A–S1C.

Two sleep pattern features are particularly disrupted in *pink1* and *parkin* mutants, and these defects are also observed in the disrupted sleep patterns of Parkinson's disease patients: (1) the anticipation of dawn and (2) the fragmentation of sleep (De Pablo-Fernández et al., 2017; Peeraully et al., 2012). Wild-type flies kept on a 12-hr dark-light cycle use their endogenous circadian rhythms to anticipate the timing of dusk or dawn, becoming more active in the 3-hr period preceding these events (Figure 1A; Chiu et al., 2010). In contrast, flies with *parkin* or *pink1* mutations fail to anticipate dawn (and to a lesser extend dusk) and remain inactive until the switch to light (Figures 1B and 1C). We confirm that the morning and evening anticipation defects are specific to *parkin* or *pink1* loss by analyzing different independently generated mutants (Figure S1D). In addition, the defects in morning and evening anticipation are also reversed by re-expressing wild-type Parkin or Pink1, but not by re-expressing mutant forms of these proteins (Figures 1B, 1C, and S1D; Clark et al., 2006; Pesah et al., 2004). Note that the presence of these genomic rescue constructs in a wild-type background does not affect any of the measured parameters. Furthermore, we also find that *parkin* and *pink1* mutant flies show normal overall locomotor activity, ruling out that our observations are the result of decreased motor ability (Figure S1E).

To further examine this circadian defect in *parkin* and *pink1* mutants, we trained the flies in 12 hr light-dark cycles for 7 days and then assessed the maintenance of circadian rhythmicity in the absence of a light cycle by keeping the flies in constant darkness. Despite the continuous darkness, wild-type flies still display a strong circadian-dependent oscillatory pattern with a bout of activity at dusk and dawn. In contrast, *parkin* and *pink1* mutants have a weaker oscillatory amplitude (Figures S1F and S1G). The circadian period, which is a direct measurement of the coordinated expression and degradation of the circadian genes and proteins (period, clock, etc.), is not altered in flies with *parkin* or *pink1* mutations (Figure 1D); however, we detect a significant decrease in the number of rhythmic flies (Figure 1E) and a loss of the circadian power (Figure 1F). These results implicate Parkin and Pink1 in the control of endogenous circadian rhythmicity through a mechanism independent of the regulation of the circadian genes.

Another prominent feature observed in Parkinson's disease patients is an inability to maintain sleep, manifested as sleep fragmentation during the night (Peeraully et al., 2012). As noted above, we find frequent awakenings (short periods of activity that are preceded and succeeded by a sleep period) in *parkin* and *pink1* mutant flies, and these occur both during the night and day (Figures 1G, 1I, 1J, and S2A–S2D). Again, we rescue these defects by re-expressing wild-type Parkin or Pink1 (Figures 1G, 1I, 1J, and S2A–S2D). The sleep fragmentation is the result of a decrease in the length of the sleep bouts and an increase in their frequency (Figures S2E–S2H). Whereas *parkin* and *pink1* mutant flies display fragmented sleep, similar to patients, their total amount of sleeping minutes (at night or during the day) is not affected (Figures 1H and S2I–S2L). We conclude that *pink1* and *parkin* mutant flies recapitulate several cardinal features of rhythmicity and sleep pattern disturbances that are also evident in Parkinson's disease.

Neuropeptidergic Neuron Defects in *parkin* and *pink1* Mutants

To define the cells responsible for the circadian rhythmicity and sleep pattern defects, we resorted to cell-type-specific $parkin^{RNAi}$ expression. We first show that $parkin^{RNAi}$ or $pink1^{RNAi}$ expression significantly lowers *parkin* or *pink1* RNA expression (Figure S2M). Organism-wide or neuron-specific $parkin^{RNAi}$ and $pink1^{RNAi}$ expression (tubulin-Gal4 or Elav-Gal4) both recapitulate the morning anticipation and brief awakening defects observed in *parkin*- and *pink1*-null mutants (Figures 2A and 2B), indicating that Parkin and Pink1 control these via a role in neurons. We further refined the defect by mapping them to specific neuronal clusters in the brain using GAL4-mediated expression of the RNAi construct in different circadian and sleep-related neuronal clusters. $parkin^{RNAi}$ or $pink1^{RNAi}$ mimics specific aspects of *parkin*- and *pink1*-null mutants when expressed in defined neuropeptidergic neurons (pigment-dispersing factor [PDF]-Gal4,

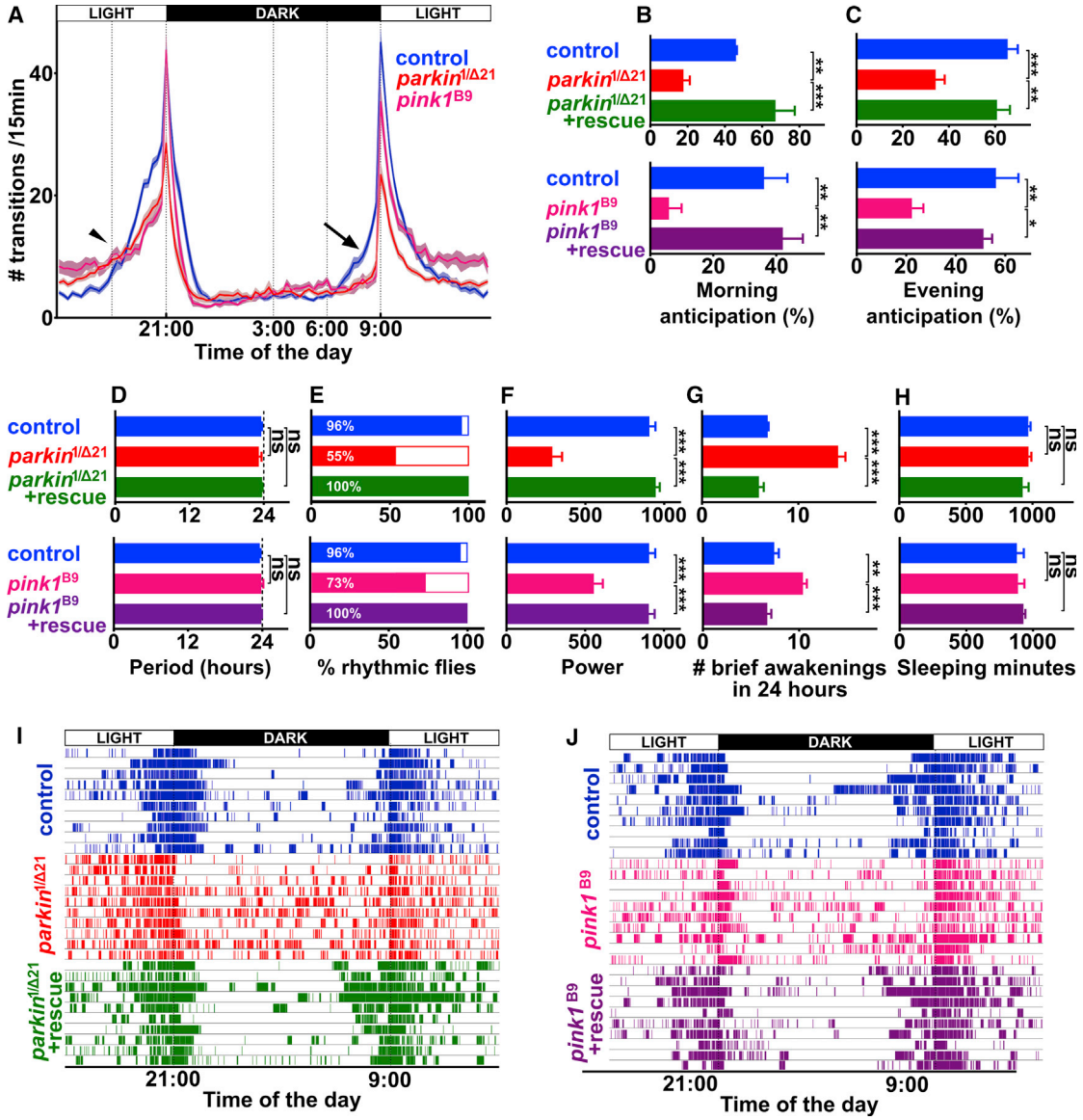

Figure 1. Circadian and Sleep Pattern Defects in *parkin* and *pink1* Mutant Flies

(A–C) 24-hr average activity plotted as the number of infrared beam breaks measured per 15 min of control, *parkin*- and *pink1*-null mutant flies (A) and quantification of morning anticipation (arrow in A; B) and evening anticipation (arrowhead in A; C). Defects in *parkin* and *pink1* mutants are rescued by a genomic fragment containing the wild-type gene. n = 3–22 assays with >25 flies per assay. *p < 0.05, **p < 0.01, and ***p < 0.001 by Bonferroni's test following one-way ANOVA. Data are represented as mean ± SEM.

(D–F) Quantification of the circadian period (D), the percentage of rhythmic flies (E), and the power of the circadian cycle (F) of controls, *parkin*, and *pink1* mutants (without and with a genomic rescue construct) entrained in a 12-hr light-12-hr dark cycle and tested in constant dark conditions. In (D) and (F), only rhythmic flies were quantified. n = 20–23 flies. ns, not significant; ***p < 0.001 by Bonferroni's test following one-way ANOVA. Data are represented as mean ± SEM.

(G–J) Quantification of the number of brief awakenings in a 24-hr period (G) and the number of sleeping minutes in a 24-hr period (H) for control flies, *parkin*, and *pink1* mutants (with or without a genomic rescue construct) and 24-hr activity plots of individual flies (rows; I and J). Each vertical bar represents an active minute. n = 5–9 assays with more than 25 flies per assay. ns, not significant, **p < 0.01 and ***p < 0.001 by Bonferroni's test following one-way ANOVA. Data are represented as mean ± SEM.

See also Figures S1 and S2.

sNPF-Gal4, Ilp2-Gal4, and c929-Gal4; Figures 2A and 2B). In particular, RNAi expression in the ventral lateral neurons (LNvs) (driven by PDF-Gal4; Figures 2A and 2B; Renn et al., 1999) prevents anticipation of dawn, whereas RNAi in insulin-producing cells (IPCs, driven by Ilp2-Gal4; Crocker et al., 2010) increases the number of brief awakenings (Figures 2A and 2B). Indicating specificity, we find very similar results by expressing two independently generated *parkin* and *pink1* RNAi lines (Figure S2N). Our observations are in line with models of how these neurons regulate the circadian cycle (LNvs; Helfrich-Förster and

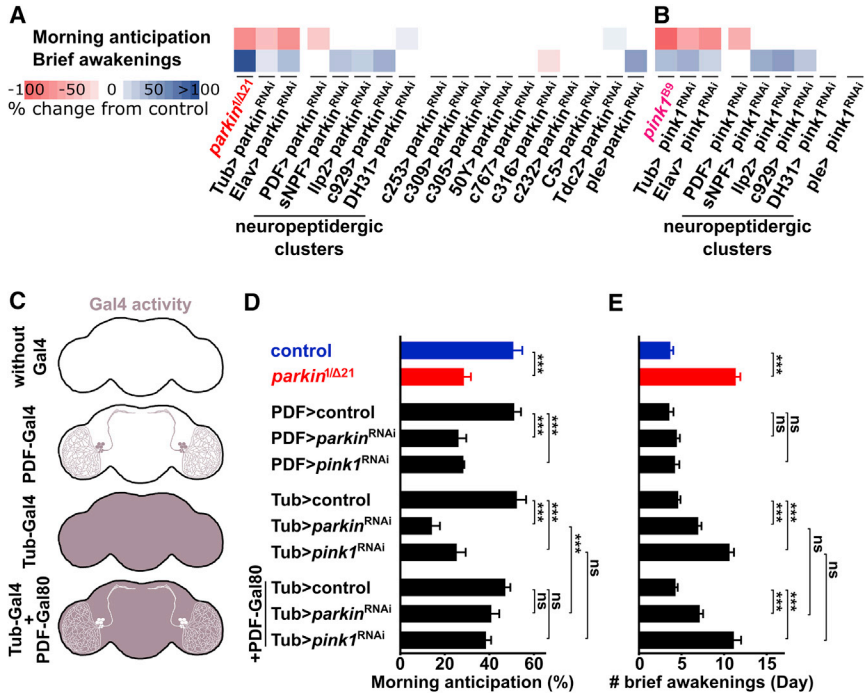

Figure 2. Parkin and Pink1 Function in Neuropeptidergic Neurons to Control Circadian Rhythms and Sleep Patterns

(A and B) Schematic representation of a mini-screen where Parkin (A) or Pink1 (B) was downregulated using RNAi and different (indicated) Gal4 lines. *parkin*- and *pink1*-null mutants are included for comparison. Shades of blue and red indicate % change from control (increase or decrease, respectively), and only significantly different changes are included ($p < 0.05$; Mann-Whitney test). Note that RNAi expression with PDF-Gal4 recapitulates the morning anticipation defect whereas several other neuronal drivers, including the Ilp2-Gal4, recapitulate the brief awakening defect (n = 3–8 assays with more than 25 flies per assay).

(C) LNv-specific requirements for Parkin and Pink1 function to elicit morning anticipation defects. Graphic representation of where Gal4 is present to drive RNAi expression. PDF-Gal4 expresses RNAi only in LNvs, and tubulin-Gal4 broadly expresses RNAi. In the presence of tubulin-Gal4, PDF-Gal80 neutralizes Gal4 activity in LNvs, whereas Gal4 is still active in the remaining neurons.

(D and E) Quantification of morning anticipation (D) and brief awakenings (E) in flies with Parkin or Pink1 downregulated in the clusters outlined in (C). Note that Pink1 and Parkin function in LNvs alone is sufficient to drive morning anticipation. n = 14–32 flies. ns, not significant and ***$p < 0.001$ by Bonferroni's test following one-way ANOVA. Data are represented as mean ± SEM.

See also Figure S2.

Homberg, 1993; Renn et al., 1999) or sleep maintenance (IPCs; Crocker et al., 2010). Indeed, we confirm that genetic ablation of the neurons using upstream activating sequence (UAS)-hid or UAS-ricin also results in decreased morning anticipation (ablation of LNvs) and increased brief awakenings (ablation of IPCs; Figures S2O and S2P). Hence, loss of Parkin or Pink1 function in specific neuropeptidergic neurons is sufficient to recapitulate aspects of the circadian and sleep pattern defects.

To determine whether Parkin or Pink1 function in the LNvs alone is sufficient to support normal morning anticipation, we removed Parkin or Pink1 function everywhere except in LNvs. We used tubulin-Gal4 to express RNAi in all cells but inhibited Gal4 activity in LNvs by expressing Gal80 (PDF-Gal80; Figure 2C; Stoleru et al., 2004). *parkin*^{RNAi}- or *pink1*^{RNAi}-expressing flies (using tubulin-Gal4) show a defect in morning anticipation and increased brief awakenings (Figure 2D), but in the presence of PDF-Gal80, the morning anticipation defect is rescued (Figure 2D). As expected, the increased brief awakenings persist in the presence of PDF-Gal80, again indicating that this defect is elicited by the loss of Parkin or Pink1 in other cells than the LNvs (e.g., IPCs; Figure 2E). These results also imply that Pink1 and Parkin elicit morning anticipation defects independent of dopaminergic neuron dysfunction. We confirm this by expression of *parkin*^{RNAi} or *pink1*^{RNAi} using the dopaminergic driver ple-Gal4 and find it does not affect the morning anticipation score (Figures 2A and 2B). This indicates morning anticipation is independent of Pink1 and Parkin function in dopaminergic cells. Conversely, we do observe a defect in brief awakenings upon *parkin*^{RNAi} expression (but not upon *pink1*^{RNAi} expression) using ple-Gal4 (Figures 2A and 2B). This is consistent with the idea that, in addition to its role in IPCs, Parkin function in dopaminergic circuits may regulate this phenotype. Nonetheless, our results indicate that Pink1 and Parkin are required in specific neuropeptidergic neurons to control circadian rhythms and sleep patterns.

Neuropeptides Are Arrested in Neuronal Cell Bodies of *parkin* and *pink1* Mutant Flies and Patient-Induced Neurons

We first looked at LNvs in more detail because knockdown of Parkin or Pink1 in these neurons causes strong phenotypes in morning anticipation score. In addition, prior studies indicated that Parkin RNA levels in LNvs are enriched 12-fold over other neurons in the fly brain (Kula-Eversole et al., 2010). Finally, Parkin and Pink1 mRNA levels oscillate with the circadian cycle, being higher at night (Kula-Eversole et al., 2010), when the LNvs actively release PDF. We therefore assessed whether *parkin* and *pink1* mutant LNvs produce PDF-loaded vesicles and transport these to the terminals. We labeled mutant brains at zeitgeber time 23 (1 hr before the lights-on event) with anti-PDF antibody (Figure 3A). This finds reduced levels of PDF at neuron terminals and increased PDF levels in cell bodies compared to controls (Figures 3B and 3C). These differences are not because of changes in PDF mRNA expression levels in the mutants as gauged by qPCR (Figure S3A). Furthermore, the PDF distribution defects are recapitulated by

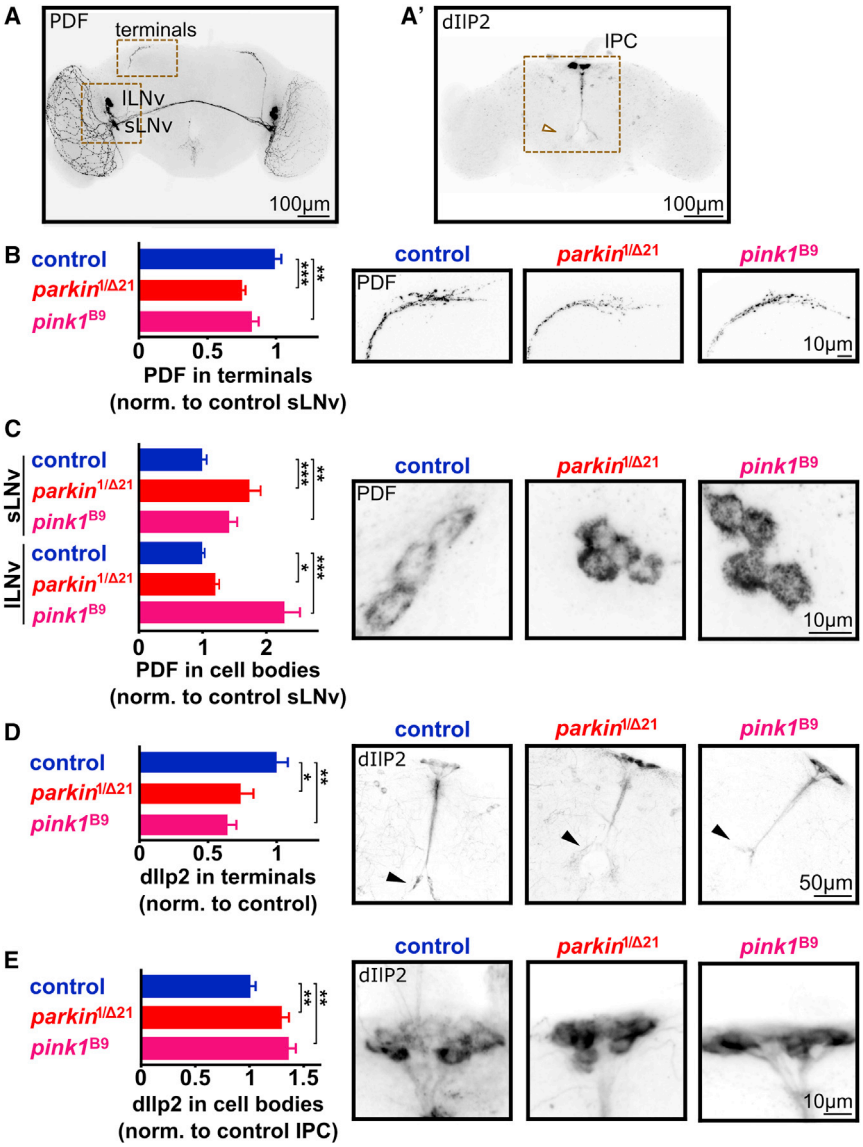

Figure 3. Neuropeptides Accumulate in the Cell Bodies of *parkin* and *pink1* Mutant Neurons

(A and A') *Drosophila* brains labeled with anti-PDF (A) or anti-dIIp2 (A'). The neuronal cell body is indicated, as are the locations of terminals (arrowhead in A'). The orange boxed areas indicate the regions that are shown in subsequent panels and figures.

(B–E) Quantification of labeling intensity and images of anti-PDF-labeled LNv terminals (B) and cell bodies (C) and dIIp2-labeled neurons (D) and cell bodies (E). Animals were dissected at zeitgeber time 23. n = 37–47 animals in (B) and (C); 25–69 animals in (D) and (E). *$p < 0.05$, **$p < 0.01$, and ***$p < 0.001$ by Bonferroni's test following one-way ANOVA. Data are represented as mean ± SEM. See also Figure S3.

RNAi-mediated downregulation of Parkin or Pink1 in LNvs, indicating the effect is cell autonomous to these neuropeptidergic neurons (Figures S3B–S3E).

Next, we analyzed the defects underlying the brief awakenings phenotype that was strongly affected in *pink1* and *parkin* mutants. Loss of Pink1 and Parkin in several neuropeptidergic neuron clusters and the loss of Parkin in the dopaminergic neurons affected this parameter (Figures 2A and 2B). We chose to analyze neuropeptide distribution in the IPCs because of their concentrated, specific localization in the brain (Figure 3A') and because we have access to specific antibodies that recognize *drosophila* Insulin-like peptide type 2 (dIIp2), produced in the IPCs (Rulifson et al., 2002). We find dIIp2 labeling is increased in the IPC cell bodies and decreased in the IPC neuron terminals (Figures 2D and 2E). Hence, both dIIp2 (in the IPCs) and PDF (in the LNvs) fail to properly localize at terminals and are retained in the cell body.

To further test the neuropeptide distribution defects, we expressed an exogenous neuropeptide, rat neuropeptide atrial natriuretic factor tagged with GFP (ANF-GFP) (Rao et al., 2001) in the LNvs or IPCs. ANF uses the fly cellular machinery to be produced and processed, and we find it is also retained in the cell bodies of the LNvs (Figure S3F) and of the IPCs (Figure S3G) of *parkin* mutant flies. Finally, the defect we observe is specific to neuropeptides because expression of synaptotagmin-GFP, a synaptic-vesicle-associated protein also produced in the cell body, distributes normally to synapses of LNvs in the mutants (Figures S3H and S3I). These data indicate that neuropeptide distribution is broadly affected in Parkinson's disease mutant flies.

Fly LNvs are analogous to neurons in the human hypothalamus, and both fly and human neurons secrete neuropeptides in the hours preceding dawn (Kunst et al., 2015; Richter et al., 2014). Human neurons secrete vasoactive intestinal peptide (VIP), whereas fly neurons secrete the VIP-like neuropeptide PDF (Vosko et al., 2007). To determine whether our findings are evolutionary conserved, we generated induced human hypothalamic neurons (Figure S4A; Merkle et al., 2015). We used two patient-derived iPSCs carrying *parkin* mutations, two patients with *pink1* mutations, and two age-matched individuals without Parkinson's disease (Figure S4B; Seibler et al., 2011; Zanon et al., 2017). We confirmed that these four patients suffered from sleep disturbances, whereas the control individuals had no complaints (Figure S4B). Differentiated hypothalamic neurons with or without *parkin* and *pink1* mutations express mature neuronal markers and neuropeptides, including VIP, a circadian coordinator in mammals (Figures 4A and S4C). Similar to the observations in flies, we find that anti-VIP immunoreactivity is lower in neurites and increased in cell bodies of the neurons derived

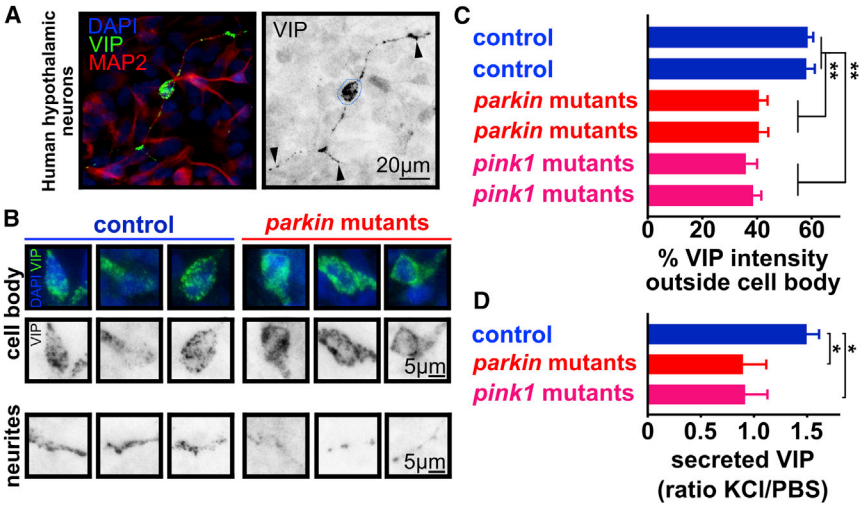

Figure 4. *parkin* and *pink1* Mutant Human Hypothalamic Neurons Release Less VIP

(A) Images of human hypothalamic neurons from induced pluripotent stem cells (iPSCs) of non-diseased people (control) labeled with DAPI (nucleus), anti-VIP, and anti-MAP2 showing VIP in the cell body (dashed circle) and in the neurites (arrows).

(B and C) Images of cell bodies and neurites of control and *parkin* mutant human hypothalamic neurons labeled with anti-VIP and DAPI (3 representative examples; B) and quantification of anti-VIP labeling intensity outside cell bodies in neurons of 2 independent controls and 4 independent Parkinson's disease patients with *parkin* or *pink1* mutations, indicating lower VIP levels in neurites of mutant cells (C). n = 22–74 cells per condition from 2 independent differentiations for all cell lines. **p < 0.01 by Bonferroni's test following one-way ANOVA. Data are represented as mean ± SEM.

(D) Quantification of VIP release into the medium measured by ELISA when neuronal cultures are chemically stimulated with 60 mM KCl. Data for control, *parkin*, and *pink1* mutant human neurons are pooled (n = 4–6 assays per condition) and normalized to measurements in non-stimulated conditions. *p < 0.05 by Bonferroni's test following one-way ANOVA. Data are represented as mean ± SEM.

See also Figure S4.

from the four patients (Figures 4B and 4C). Consistently, ELISA-based measurements of extracellular VIP show that the induced hypothalamic neurons from these patients also secrete less VIP into the medium than control cells when the neurons are chemically stimulated (Figure 4D). Hence, VIP delivery to synapses in *parkin* or *pink1* mutant human neurons is impaired, also causing a defect in the coordinated release of this neuropeptide.

Neuropeptides Are Arrested in the ER of Parkinson's Disease Mutant Neuropeptidergic Cells

Neuropeptides are produced in the ER and then transported through the Golgi network and loaded in dense core vesicles (DCVs) that are finally transported to the release sites. The increased labeling of neuropeptides in the cell body of *parkin* or *pink1* mutant neurons can be explained either by a defect in trafficking of DCVs to their release sites, resulting in the accumulation of DCVs in cell bodies or by the retention of neuropeptides in the ER-Golgi complex, e.g., as a result of a defect to produce DCVs.

To analyze DCV number and location in LNvs in the brain, we used correlative 3D Block face scanning electron microscopy. We labeled LNvs with anti-PDF antibody coupled to horseradish peroxidase (HRP) that converts diaminobenzidine (DAB) into a precipitate visible by electron microscopy (EM) (Figures S5A–S5D). Cell bodies of LNvs were then reconstructed, and DCVs were identified based on morphology. The number of DCVs is significantly lower in cell bodies of *parkin* mutants (Figures 5A and S5E). Hence, despite the increased levels of PDF in *parkin* mutant LNv cell bodies, we find less DCVs. These data are consistent with a requirement for Parkin in the production of DCVs.

Neuropeptide packaging and trafficking is coupled to their post-translational processing while they transfer from the ER to the Golgi into DCVs (Loh, 1987). To directly assess neuropeptide processing, we expressed dIlp2-GFP in the IPC neurons and performed western blotting to detect immature and mature forms of dIlp2 (the GFP moiety facilitates detection on western blotting). dIlp2-GFP is produced as an immature pre-pro-neuropeptide in the ER and is then consecutively cleaved by the fly machinery to the fully processed form that resides in DCVs (Arvan and Castle, 1998; Brogiolo et al., 2001). Consistent with our observation of decreased DCV number *parkin* mutants, we find a significant accumulation of immature uncleaved dIlp2-GFP (approximately [approx.] 42 kDa) and a decrease in the partially (approx. 39 kDa) and fully processed dIlp2-GFP (approx. 31 kDa; Figures 5C and 5D). We independently confirm this result by expressing ANF-GFP in *parkin* mutants, where we also observe an increased amount of unprocessed and partially processed ANF-GFP at the expense of the fully processed form (Figures S5F and S5G; Rao et al., 2001). These data are consistent with reduced DCV formation in *parkin* mutants.

Increased ER-Mitochondrial Contacts in *parkin* and *pink1* Mutant Neuropeptidergic Neurons

We next wondered how the function of Parkin and Pink1 could connect to DCV formation. Pink1 recruits Parkin to mitochondria, where it ubiquitinates proteins (Geisler et al., 2010). In some cell types, the loss of *parkin* or *pink1* results in morphologically abnormal mitochondria (Esposito et al., 2013; Pesah et al., 2004). However, in many other cell types, including several types of neurons in flies, mice, and patients, chronic loss of *parkin* and *pink1* does not cause overt mitochondrial morphological defects (Burman et al., 2012; Clark et al., 2006; Damiano et al., 2014; Gautier et al., 2008; Morais et al., 2009; Pickrell and Youle, 2015). We therefore labeled mitochondria by expressing mito-GFP in LNvs or with an antibody targeting TOM20 in human hypothalamic neurons with *parkin* or *pink1* mutations. This did not reveal significant changes in mitochondrial volume or mitochondrial morphology between the mutant cells and control cells (Figures S5H–S5J). We also assessed mitochondrial morphology in LNvs using electron microscopy. This does not reveal obvious

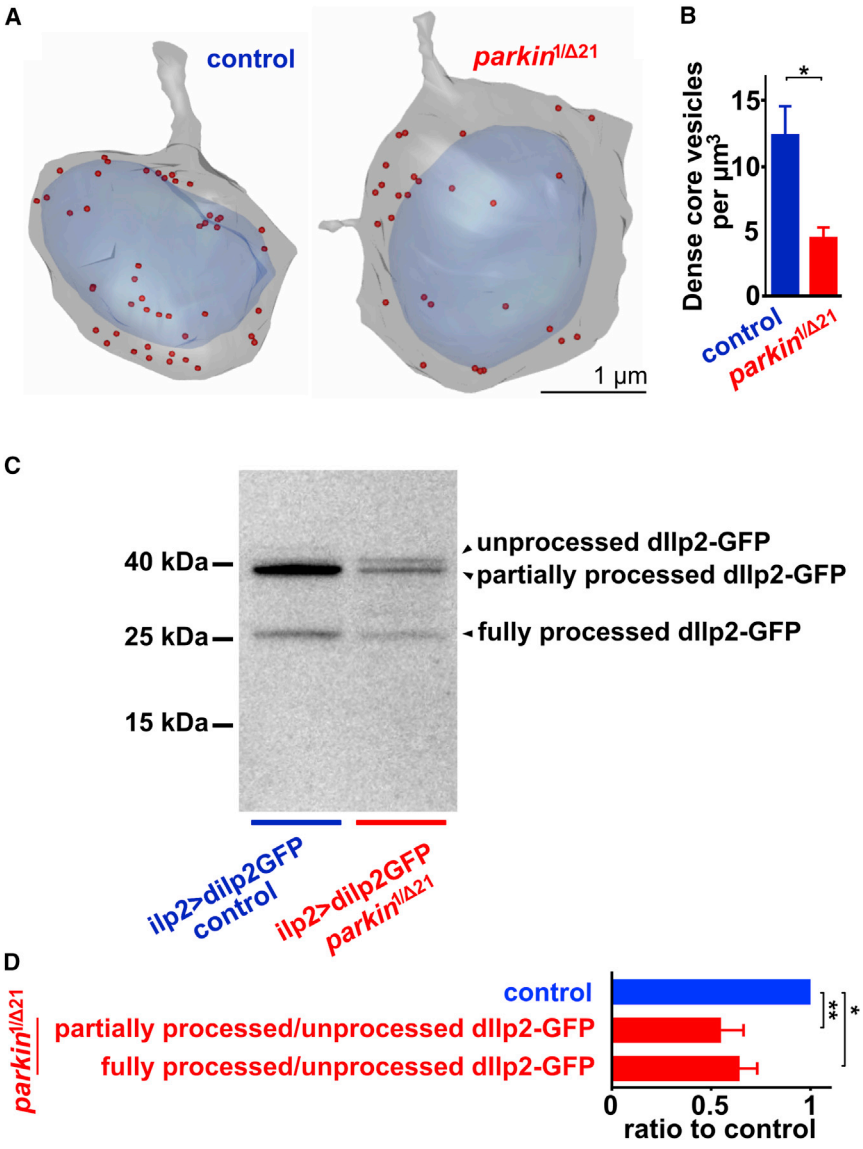

Figure 5. Dense Core Vesicle Number and Neuropeptide Processing Are Decreased in LNvs of *parkin* Mutants

(A and B) 3D reconstructions of PDF-HRP-labeled LNv cell bodies using focused ion beam scanning electron microscopy (FIB-SEM) stacks, indicating the nucleus (blue), the cytoplasm (gray), and DCVs (red) in control fly and a *parkin* mutant fly (A) and quantification of the number of DCVs per cellular volume (B). For all quantifications, we ensured the nucleus and the large majority of the cell body was present in our reconstructions. n = 6 or 7 reconstructions from 4 control and 4 *parkin* mutant brains. *p < 0.05 by Mann-Whitney test.

(C and D) Western blot of adult fly heads expressing dIlp2-GFP in IPCs under control of Ilp2-Gal4 in control and *parkin* mutant flies probed with anti-GFP. The bands for unprocessed, partially processed, and fully processed dIlp2-GFP are indicated (C) and the quantification of the intensity of each band normalized to the unprocessed neuropeptide (D). n = 4 independent experiments. *p < 0.05 and **p < 0.01 by Bonferroni's test following one-way ANOVA. Data are represented as mean ± SEM.

See also Figure S5.

abnormalities in cristae structure in the LNvs of *parkin* mutants (Figure S5K).

Proteins ubiquitinated by Parkin are typically sent for degradation, and an inability to ubiquitinate them leads to elevated levels of these Parkin targets both in *parkin* and *pink1* mutants. This has been observed for mitofusin (*Drosophila* MARF), VDAC (*Drosophila* porin), and Miro (Geisler et al., 2010; Poole et al., 2010; Wang et al., 2011). Interestingly, several of these targets are proteins that stabilize ER-mitochondrial contact sites (Figure S6A; de Brito and Scorrano, 2008; Erpapazoglou and Corti, 2015; Helle et al., 2013; Poston et al., 2013). Consistently, the loss of *parkin* has been shown to result in more ER-mitochondrial contacts (Celardo et al., 2016; Gautier et al., 2016), but this was not tested in LNvs *in vivo*. We imaged fluorescently labeled ER and mitochondria in LNv and IPC cell bodies to evaluate the distance distribution between these organelles (see STAR Methods). This analysis indeed finds a significant increase in the contact surface between these organelles in LNvs and IPCs of *parkin* and *pink1* mutants (Figures 6A–6D, S6B, and S6C). Similarly, we also find an increase in the ER-mitochondrial contact surface when we overexpress the Parkin target MARF in LNvs, indicating that the upregulation of Parkin targets is sufficient to generate more contacts (Figure S6D). We independently confirm the contact surface is increased based on volume reconstructions of our 3D EM data stacks of *parkin* mutant LNv cell bodies, where we highlight areas where ER and mitochondria are within a distance of <30 nm in yellow (Figure 6E). These data indicate that the loss of Parkin activity promotes the formation of ER-mitochondrial contacts in fly LNvs.

To determine whether the increased ER-mitochondrial contact surface is evolutionary conserved, we resorted to our induced hypothalamic neurons differentiated from patient iPSCs. We used antibodies to label ER (anti-protein disulfide-isomerase [PDI]) and mitochondria (anti-TOM20) and also find an increased contact surface between ER and mitochondria in mutant neurons (Figures 6F, 6G, and S6E). Hence, both in mutant fly LNvs and IPCs, as well as in induced neuropeptidergic neurons from Parkinson's disease patients, the contact surface between ER and mitochondria is increased.

Increased ER-Mitochondrial Contacts Cause Morning Anticipation Defects in *Drosophila*

Our data suggest that defects to produce PDF-loaded DCVs in the ER-Golgi system cause circadian defects. We therefore

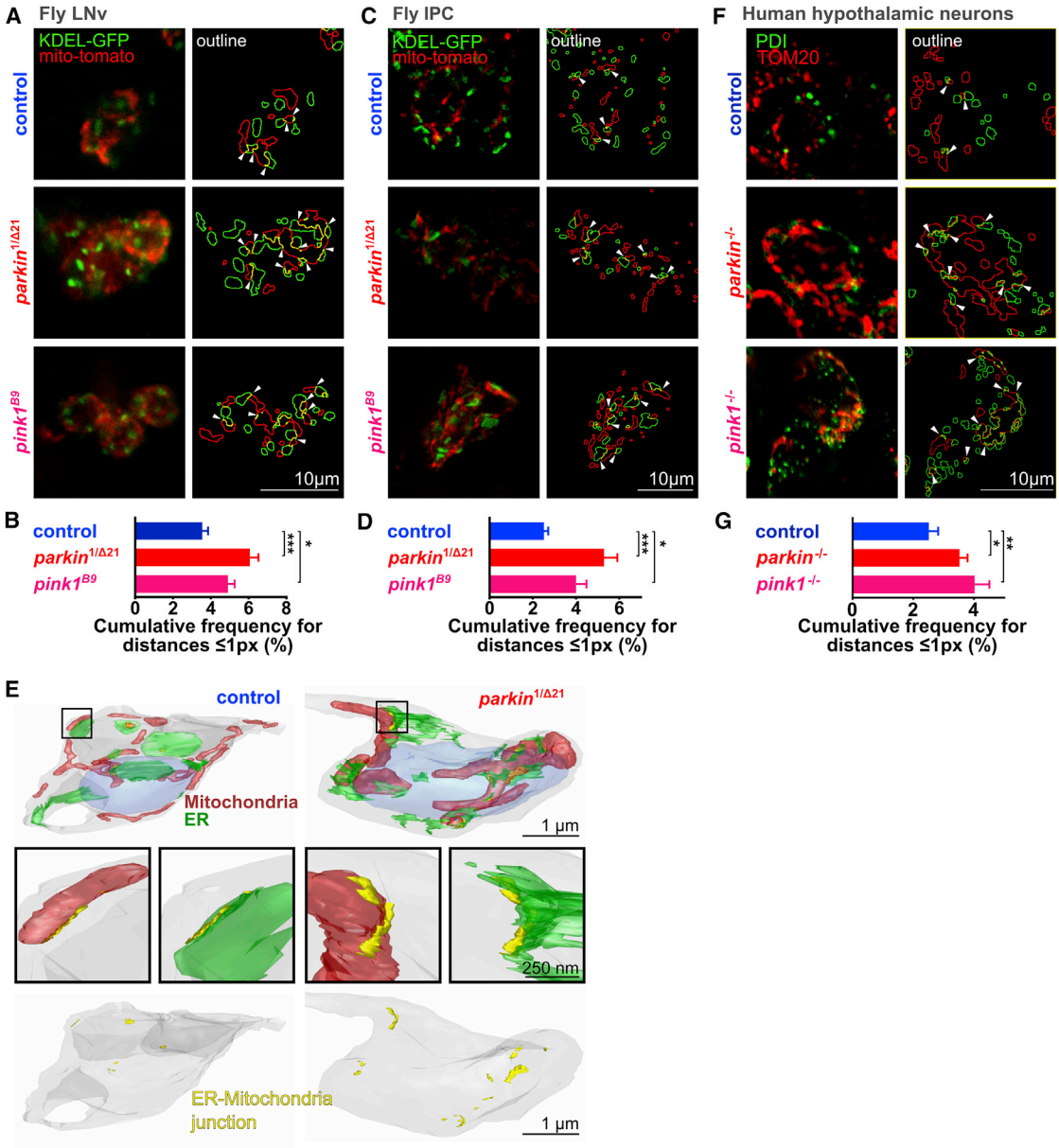

Figure 6. ER-Mitochondria Contacts Are Increased in *parkin* and *pink1* Mutant Neuropeptidergic Neurons

(A–D) Images of LNv cell bodies (A) and IPC neuron cell bodies (C) that express KDEL-GFP (ER, green) and mito-tdTomato (mitochondria, red) of controls, *parkin*, and *pink1* mutants (A and C, left) and the outline of ER and mitochondria labeling, where arrowheads indicate where the labeling connects (A and C, right). Quantification of the extent of the contacts between ER and mitochondria in LNv (B) and IPC (D) cell bodies of *parkin* and *pink1* mutants (e.g., quantification of the frequency of ER pixels within a distance of one pixel from mitochondria). n = 7–9 brains for (B) and 16–24 brains for (C) per condition. *$p < 0.05$ and ***$p < 0.001$ by Bonferroni's test following one-way ANOVA. Data are represented as mean ± SEM.

(E) 3D model of an LNv cell body generated from a FIB-SEM data stack of a control and a *parkin* mutant fly indicating ER (green), mitochondria (red), and the contacts between them (locations where the organelles are <30 nm apart, yellow). Nucleus, blue; cytoplasm, gray; box, inset.

(F and G) Images of induced hypothalamic neurons of controls, *parkin*, and *pink1* mutant patients (F, left) labeled with anti-PDI (ER, green) and anti-TOM20 (mitochondria, red) and the outline of ER and mitochondria labeling, where arrowheads indicate where the labeling connects (F, right). Quantification (G) of the extent of the contacts between ER and mitochondria in control, *parkin*, and *pink1* mutant hypothalamic differentiated neurons. n = 16–20 neurons per genotype from two independent differentiations. *$p < 0.05$ and **$p < 0.01$ by Bonferroni's test following one-way ANOVA. Data are represented as mean ± SEM.

See also Figure S6.

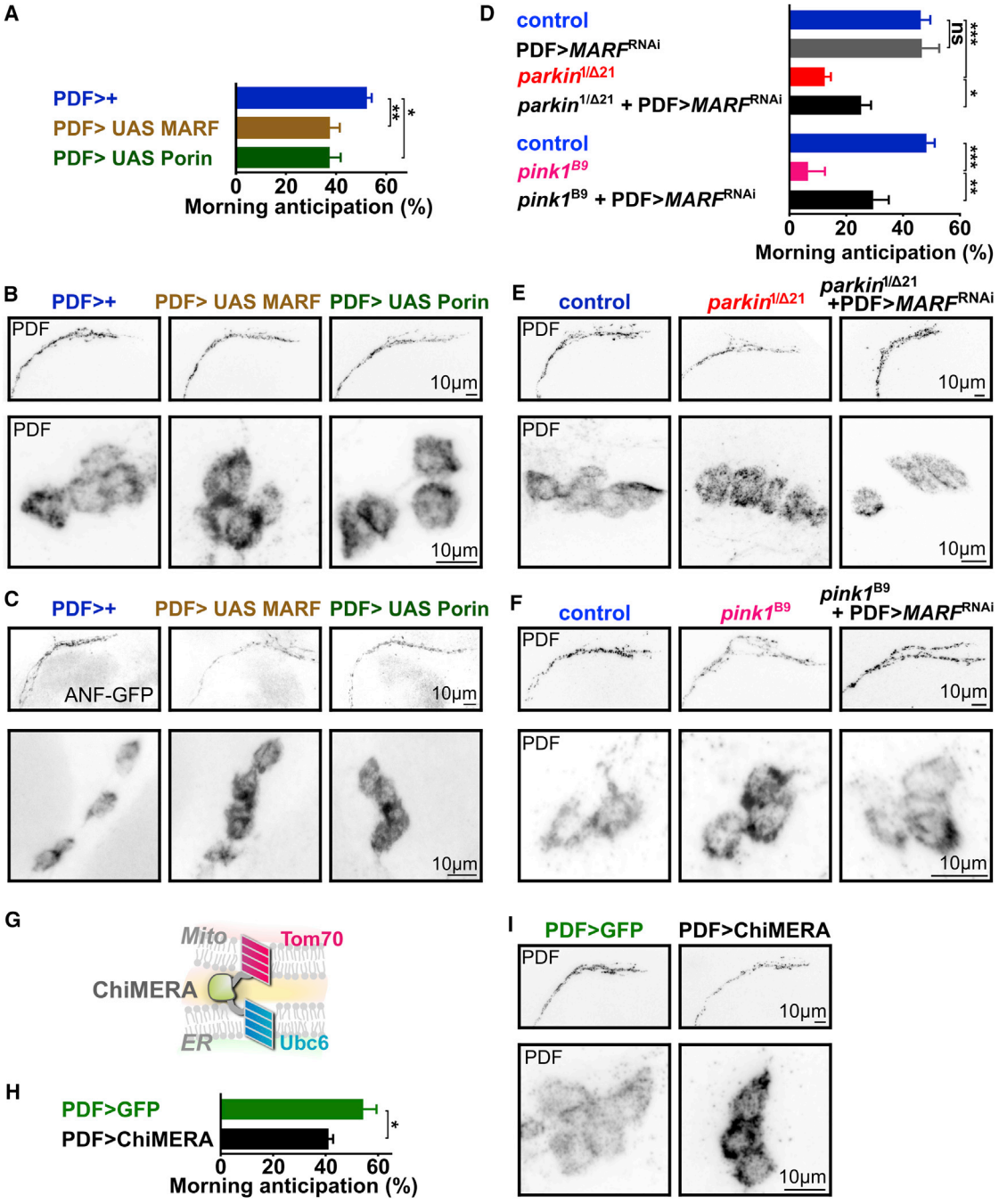

Figure 7. Increased ER-Mitochondria Contacts in *parkin* and *pink1* Mutants Are Causal to Morning Anticipation Defects

(A) Quantification of morning anticipation upon overexpression of MARF or porin in LNv (PDF-Gal4). n = 4–6 assays with 25 flies each. *p < 0.05 and **p < 0.01 by Bonferroni's test following one-way ANOVA. Data are represented as mean ± SEM.

(B and C) Images of LNv neuronal terminals and cell bodies of animals overexpressing MARF or porin in LNv (PDF-Gal4) and labeled with anti-PDF (B) or also expressing ANF-GFP, where GFP was imaged (C). Note the increased neuropeptide labeling in the cell bodies and reduced labeling at terminals. Quantification is shown in Figures S7A–S7D.

(D) Quantification of morning anticipation upon downregulation of *MARF* in LNv (PDF-Gal4) of *parkin* and *pink1* mutants. Note that this rescues the defects of *parkin* and *pink1* mutants. n = 4–6 assays with 25 flies each. ns, not significant, *p < 0.05, **p < 0.01, and ***p < 0.001 by Bonferroni's test following one-way ANOVA. Data are represented as mean ± SEM.

(E and F) Images of LNv neuronal terminals and cell bodies upon downregulation of *MARF* in LNv (PDF-Gal4) of *parkin* (E) and *pink1* (F) mutants, labeled with anti-PDF. Note that this rescues the defects of *parkin* and *pink1* mutants. Quantification is shown in Figures S7E–S7H.

(G) ChiMERA bridges the mitochondrial and ER membrane to induce additional contacts between these organelles.

(legend continued on next page)

determined whether the increased ER-mitochondria contacts we observe in *parkin* and *pink1* mutants are causal to morning anticipation defects. We started by overexpressing MARF (or porin) in LNvs of wild-type flies where ER-mitochondrial contacts are increased (Figure S6D). This causes PDF retention in cell bodies and decreases morning anticipation, very similar to our observations in *parkin* or *pink1* mutants (Figures 7A, 7B, S7A, and S7B). Similarly, when we express ANF-GFP that marks DCVs and colocalizes with PDF (Figure S7J) in the flies that overexpress MARF or porin, the ANF-GFP accumulates in LNv cell bodes at the expense of localizing to terminals (Figures 7C, S7C, and S7D). Conversely, we knocked down the Parkin target MARF (Figure S7I) in *parkin* or *pink1* mutants and find this partially rescues the PDF accumulation in the cell body as well as the defect in morning anticipation (Figures 7D–7F and S7E–S7H). Our attempts to also test another target (porin) failed, as we were unable to generate the flies. These genetic interactions are consistent with increased ER-mitochondrial contacts to cause the circadian defects we observed in *parkin* and *pink1* mutants.

To provide further evidence for a specific role of ER-mitochondrial contact sites in the regulation of morning anticipation, we created transgenic flies that express "ChiMERA," where ER-mitochondrial contacts are upregulated without the confounding factors that may arise from overexpression of endogenous proteins, such as MARF or porin. The ChiMERA protein consists of the yeast TOM70 mitochondrial membrane protein fused to the yeast ER protein, Ubc6, and GFP (Figures 7G, S7K, and S7L; Kornmann et al., 2009). Similar to the overexpression of MARF or porin, this tool drives ER-mitochondrial contact formation (Kornmann et al., 2009). Interestingly, expression of ChiMERA in LNvs causes a decrease in morning anticipation (Figure 7H). Furthermore, expression of ChiMERA results in the increased retention of PDF in LNv cell bodies and in lower levels of this neuropeptide in the LNv terminals (Figures 7I, S7M, and S7N). Hence, ER-mitochondrial contacts drive circadian rhythm defects similar to those observed in Parkinson's disease models.

Excessive Phosphatidylserine Transfer at ER-Mitochondrial Contacts Cause Circadian Rhythm and Sleep Pattern Phenotypes in *parkin* and *pink1* Mutants

ER-mitochondrial contacts are involved in different cellular processes, such as Ca^{2+} export from ER to mitochondria, generation of autophagic membranes, facilitation of the ER stress response, regulation of apoptosis, and also the transport of phosphatidylserine (PtdSer) from the ER to mitochondria, where it is metabolized to phosphatidylethanolamine (PtdEtn) (Figure S8A; Area-Gomez, 2014; Paillusson et al., 2016). Whereas we did not find evidence for a role of ER-calcium and stress in the generation of DCVs in the literature, PtdSer has been reported to be enriched in DCV membranes (Kim et al., 2014; Westhead, 1987). Based on this, we hypothesized that the increased ER-mitochondrial contact sites in the Parkinson's disease mutants affect DCV production via effects on lipid membrane composition, without excluding potential other ER-related processes that may be at play as well.

To examine the lipidome of ER-Golgi- and mitochondria-enriched membranes purified from *parkin* mutants and controls, we used shotgun lipidomics. Our mitochondria-enriched fraction presents high levels of the mitochondria-resident protein ATP synthase, whereas the ER-Golgi-enriched fraction has high levels of calreticulin, a protein in the ER lumen (Figures S8B and S8C). Both fractions only have residual levels of Discs large (DLG), a postsynaptic marker (Figure S8C), indicating that our fractions are relatively pure. The protein-to-lipid ratio and the mitochondrial and ER-Golgi concentrations of phosphatidylcholine (PtdCho) are similar in controls and mutants (Figures 8A and S8D). However, the mitochondrial fraction of *parkin* mutants contains significantly more PtdSer and PtdEtn than the mitochondrial fraction of controls, whereas the ER fraction of *parkin* mutants contains comparatively less PtdSer and PtdEtn than the ER fraction of controls (Figure 8A). This is in accordance with the increased ER-mitochondria contacts that facilitate the transfer of PtdSer from ER to mitochondria in *parkin* mutants. Mitochondrial enzymes then convert PtdSer to PtdEtn, and this creates a "PtdSer sink."

We independently confirmed the importance of ER-mitochondrial contacts to deplete PtdSer from ER by expressing ChiMERA in otherwise wild-type flies. This manipulation is sufficient to drive a similar lipid profile to the one we detect in *parkin* mutants (Figure 8A), further indicating that an increase in ER-mitochondrial contacts is sufficient to cause the lipid distribution defects in *parkin* mutants. Thus, the data indicate that increased ER-mitochondrial contacts in *parkin* mutants or in ChiMERA-expressing flies mediate excess PtdSer transfer to mitochondria and the relative depletion of PtdSer from the ER.

Next, we tested whether PtdSer levels can affect circadian rhythms. We knocked down the ER-resident enzyme PtdSer synthase with RNAi in LNvs (Figure S8E) and find that this manipulation causes a retention of PDF in the LNv cell bodies and a reduction of this neuropeptide at the terminals (Figures 8B, S8F, and S8G). Furthermore, knocking down PtdSer synthase also is sufficient to cause a defect in morning anticipation (Figure 8C) that is similar to that in *parkin* mutants. These data provide further evidence that a decrease in PtdSer levels in the ER-Golgi of *parkin* mutants can explain the phenotype we observe.

To test our model further, we also performed a rescue experiment and supplemented fly food with PtdSer. After three days of continued PtdSer feeding, the circadian and sleep defects of *parkin* and *pink1* mutants improved: both morning anticipation (Figure 8D) and brief awakenings (Figure S8H). Furthermore, after 4 days of PtdSer feeding, the altered distribution of PDF and

(H) Quantification of morning anticipation upon ChiMERA overexpression in LNv (PDF-Gal4). Note this phenocopies *pink1* and *parkin* mutants. n = 5–8 assays with 25 flies each. *$p < 0.05$ by Mann-Whitney test. Data are represented as mean ± SEM.

(I) Images of LNv neuronal terminals and cell bodies upon overexpression of ChiMERA in LNv (PDF-Gal4) labeled with anti-PDF. Note the increased neuropeptide labeling in the cell bodies and reduced labeling at terminals. Quantification is shown in Figures S7M and S7N.

See also Figure S7.

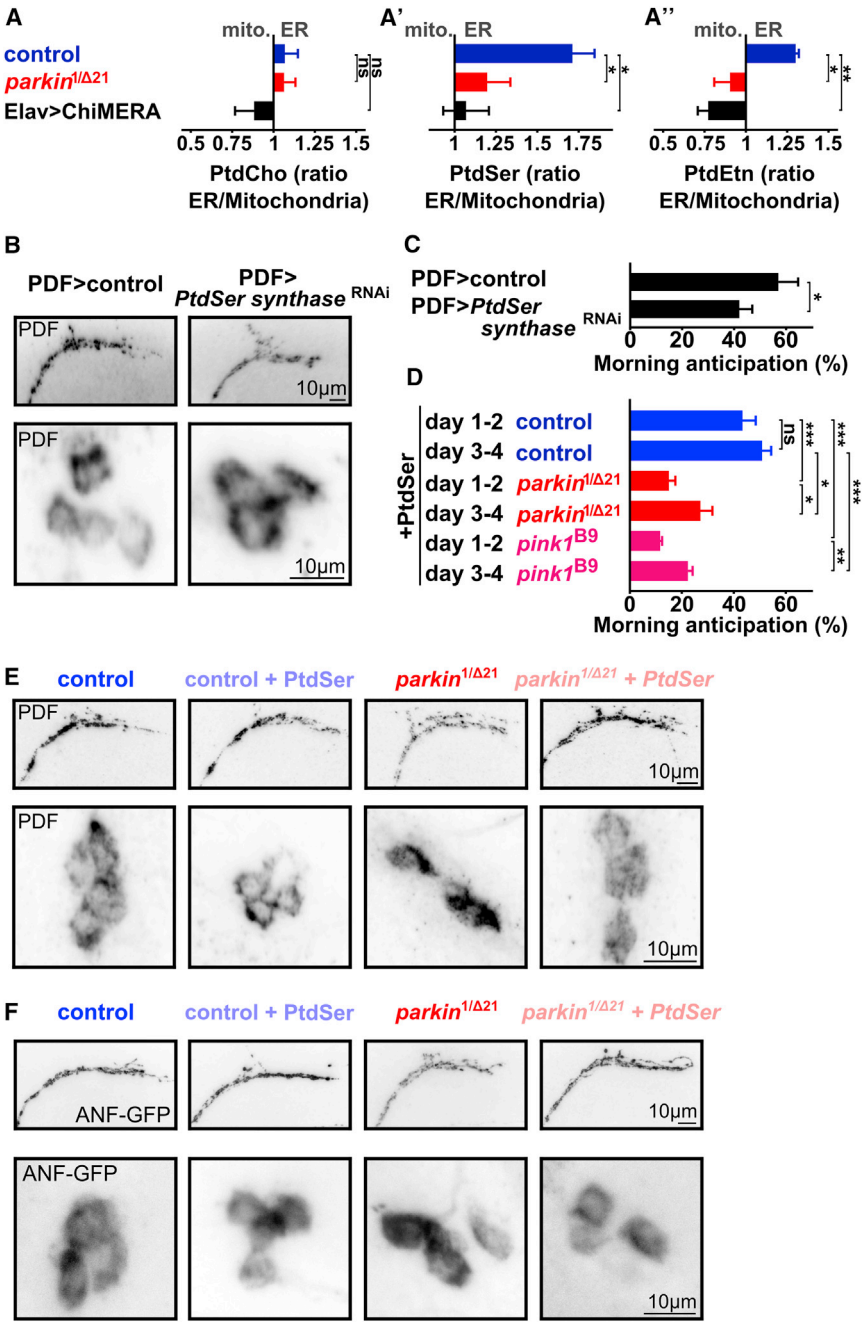

Figure 8. PtdSer Depletion from the ER Is Causative to Circadian and Sleep Pattern Defects

(A) Ratio of the amount of phosphatidylcholine (PtdCho) (A), phosphatidylserine (PtdSer) (A'), and phosphatidylethanolamine (PtdEtn) (A'') measured by mass spectrometry (MS) shotgun lipidomics in the ER fraction to the amount measured in the mitochondrial fraction of heads of control flies, *parkin* mutant flies, and flies expressing ChiMERA in neurons (Elav > ChiMERA). A ratio of 1 (indicated by the line) means the concentrations of the indicated lipid in ER and mitochondria are identical. A ratio above 1 indicates enrichment in the ER, and a ratio below 1 indicates enrichment in the mitochondria. n = 3–5 independent assays (fly collection and MS). *p < 0.05, **p < 0.01 by Bonferroni's test following one-way ANOVA. Data are represented as mean ± SEM.

(B) Images of LNv neuronal terminals and cell bodies upon expression of RNAi to PtdSer synthase in LNv (PDF-Gal4) labeled with anti-PDF. Note the increased neuropeptide labeling in the cell bodies and reduced labeling at terminals. Quantification is shown in Figures S8F and S8G.

(C) Quantification of morning anticipation upon expression of RNAi for PtdSer Synthase in LNv (PDF-Gal4). Note this phenocopies *pink1* and *parkin* mutants. n = 4 assays with 25 flies each. *p < 0.05 by Mann-Whitney test. Data are represented as mean ± SEM.

(D) Quantification of morning anticipation upon feeding control, *parkin*, and *pink1* mutant flies PtdSer 150 μM (final concentration in the food). Data for the first two days of feeding (days 1 and 2) were pooled, and data for the consecutive two days of feeding (days 3 and 4) were pooled. Note that, after 3 or 4 days of feeding, the morning anticipation defect is partially rescued, as is the defect in brief awakenings (shown in Figure S8H). Longer periods of feeding do not yield stronger rescue of the morning anticipation phenotype (not shown). n = 7 assays with 25 flies each. *p < 0.05, **p < 0.01, and ***p < 0.001 by Tukey's test following two-way ANOVA.

(E and F) Images of LNv neuronal terminals and cell bodies upon feeding control and *parkin* mutant flies PtdSer 150 μM (final concentration in the food) for 4 days, labeled with anti-PDF (E), or expressing ANF-GFP, where GFP was imaged (F). Quantification is shown in Figures S8I–S8L. Note the rescue of neuropeptide distribution upon PtdSer feeding. Similarly, PtdSer feeding also rescues dIlp2-GFP distribution defects in the IPCs (see Figures S8M and S8N).

See also Figure S8.

ANF-GFP in the LNvs of these *parkin* mutants is indistinguishable from the distribution we observe in controls fed or not fed with PtdSer (Figures 7E, 7F, and S8I–S8L). Similarly, dIlp2 distribution in the IPC neurons of *parkin* mutants fed with PtdSer is also rescued to control levels (Figures S8M and S8N). As a control, we also fed *parkin* and *pink1* mutants with PtdCho. However, here, we do not observe a rescue of brief awakenings or morning anticipation defects (Figures S8O and S8P). This result indicates PtdSer depletion specifically is the basis of the circadian and sleep pattern defects in *parkin* and *pink1* mutants.

DISCUSSION

Our data provide neurobiological, cellular, and molecular explanations for circadian and sleep pattern impairments in Parkinson's disease—a clinically well-recognized but mechanistically

not understood phenomena. The data here show that the well-known mitochondrial Parkinson's disease pathology in some of the genetic forms of the disease bifurcates in the cell at the level of the ER-mitochondrial contacts to affect other organelles like DCVs. These ER-mitochondrial contacts are central in aspects of lipid metabolism, and we find here that the lack of PtdSer, for not yet fully clarified reasons, affects the maturation of dense core vesicles in induced neurons from patients and in fly mutants.

It is a conundrum why the manifestation of phenotypes in neurodegenerative diseases caused by mutations in a single gene does not follow simply the level of the affected protein expression, i.e., not all cells respond in the same way to the presence of a mutated protein. Our data here suggest that understanding the basic cell biology is key: proteins express their function in the context of cells. We find that *parkin* and *pink1* mutations in a set of neuropeptidergic neurons affect the boost of VIP secretion that needs to happen in the hours preceding dawn and possibly other peptides important for sleep pattern regulation as well. In fact, our mini-screen showed that knockdown of Parkin or Pink1 in other neuronal clusters also elicited sleep pattern phenotypes, sometimes even in opposite directions (e.g., DH31, Tdc2, or c316), but further work will be needed to elucidate their roles in the regulation of this process. Nonetheless, our data are consistent with the normal, basal DCV production to occur normally in these cells, but the massive and fast up-regulation of DCV production that is required in a limited time window (at night) is impaired. It is clear that the particular function of these neurons makes them vulnerable to a, at first glance relatively mild, deficit in lipid metabolism that affects DCV formation. It is likely that this stabilization of ER-mitochondrial contacts may have different consequences for other cell types, and further work is needed to evaluate to what extent this alteration might activate other pathogenic stress pathways.

Sleep pattern and circadian defects and other non-motor symptoms of Parkinson's disease are relatively understudied compared to the dopaminergic neuron loss and concomitant motoric defects (Munhoz et al., 2015). Part of the reason may be that murine models of familial and sporadic Parkinson's disease do not recapitulate the sleep pattern defects seen in patients (Fifel et al., 2016). We also tested *pink1* mutant mice using 24-hr activity monitoring but failed to detect consistent defects. We resorted to fruit flies that do recapitulate cardinal features of sleep pattern and circadian disturbances of Parkinson's disease. We believe this is warranted because we were able to recapitulate all the cellular defects seen in fly neuropeptidergic neurons and also in induced hypothalamic neurons from different patients that we show also display sleep defects. Moreover, the cellular and molecular substrates that regulate circadian rhythmicity and the mechanisms of sleep are evolutionary well-conserved, and several aspects were originally discovered in flies (Hendricks and Sehgal, 2004).

A growing number of pathologies feature excess ER-mitochondrial contacts, for instance, familial Alzheimer's disease (AD), amyotrophic lateral sclerosis (ALS), Huntington's disease (HD), and type 2 diabetes mellitus (Krols et al., 2016). Interestingly, as in Parkinson's disease, also AD, ALS, and HD have marked and penetrant sleep pattern and circadian rhythmicity symptoms (Ahmed et al., 2016; Morton, 2013; Peter-Derex et al., 2015). However, little is known about the defective cellular and molecular mechanisms at the basis of these sleep pattern defects in these different neurodegenerative diseases. Our study now provides a new direction that can be tested in the context of those diseases as well, by evaluating the processing and release of sleep-pattern-controlling neuropeptides. In this context, our findings are exciting, because it is known that ER-mitochondrial contacts in other cell types than neuropeptidergic neurons can adapt quickly to the needs of the cell (Prudent et al., 2015). Our work suggests that, through its ubiquitination activity, Parkin can "quickly" regulate the prevalence of these sites in neuropeptidergic neurons as well, as to support the boost in DCV production needed at the hours preceding dawn.

Our findings have important clinical implications. Most importantly, the circadian and sleep pattern defects in Parkinson's disease are apparently caused—at least in part—by a different pharmacology than dopaminergic dysfunction, which underlies the well-known motoric dysfunction. Indeed, sleep dysfunction in Parkinson's disease is not rescued by dopamine replacement therapy (Lee and Koh, 2015). In addition, our genetic work is in further support of this, as we show that, when *parkin* or *pink1* are knocked down everywhere (also in the dopaminergic neurons), except in the LNvs, such animals do not show a defect in morning anticipation. It is also important to note that the disordered circadian rhythmicity and sleep patterns are caused by neuronal dysfunction and not neurodegeneration, which implies that it can be corrected, as we show here in flies by the addition of PtdSer to the food.

STAR★METHODS

Detailed methods are provided in the online version of this paper and include the following:

- KEY RESOURCES TABLE
- CONTACT FOR REAGENT AND RESOURCE SHARING
- EXPERIMENTAL MODEL AND SUBJECT DETAILS
  - Fly stocks and maintenance
  - iPSC maintenance and differentiation
- METHOD DETAILS
  - Fly activity assay
  - *Drosophila* neuropeptide distribution and mitochondria morphology
  - Staining in human differentiated neurons
  - Neuropeptide secretion
  - ER-mitochondria distance in flies
  - Western blotting
  - Electron microscopy
  - Quantitative real-time PCR
  - Lipid measurement in ER and mitochondrial fractions
  - Lipid supplemented food experiment
- QUANTIFICATION AND STATISTICAL ANALYSIS
  - Statistical Analysis

SUPPLEMENTAL INFORMATION

Supplemental Information includes eight figures and can be found with this article online at https://doi.org/10.1016/j.neuron.2018.05.022.

ACKNOWLEDGMENTS

We thank the Bloomington, Harvard, and Kyoto *Drosophila* stock centers and the Developmental Studies Hybridoma bank as well as Bart De Strooper, Patrick Callaerts, Sha Liu, Edwin S. Levitan, Wim Vandenberghe, and Rose Goodchild for reagents. We thank Bart De Strooper, Sha Liu, Wim Vandenberghe, Georg Halder, Vanessa A. Morais, Rose Goodchild, Joseph McInnes, Sabine Kuenen, António Laranjeira, Elsa Lauwers, Ana Rita Santos, the VIB BioImaging core facility, and all members of the Verstreken lab for discussions and help. This work was supported by an ERC Consolidator Grant (646671), the FWO Vlaanderen, the Hercules Foundation, IWT, BELSPO-IAP, a Methusalem grant of the Flemish government, Opening the Future, the Vlaamse Parkinsonliga, and VIB. J.S.V. is supported by the Fundação para a Ciência e a Tecnologia (FCT, grant number SFRH/BD/88363/2012), D.V. is supported by the FWO Vlaanderen, and P.V. is a member of the FENS Kavli Network of Excellence.

AUTHOR CONTRIBUTIONS

J.S.V., G.E., D.V., K.M., L.D., and S.R. performed research and/or analyzed the data. J.S.V., G.E., K.M., and P.V. designed experiments. P.S. and C.K. provided iPSCs. J.S.V. and P.V. made the figures, wrote the paper, and conceptualized the study. All authors discussed the results and commented on the manuscript.

DECLARATION OF INTERESTS

The authors declare no competing interests.

Received: December 18, 2017
Revised: April 16, 2018
Accepted: May 14, 2018
Published: June 7, 2018

REFERENCES

Ahmed, R.M., Newcombe, R.E.A., Piper, A.J., Lewis, S.J., Yee, B.J., Kiernan, M.C., and Grunstein, R.R. (2016). Sleep disorders and respiratory function in amyotrophic lateral sclerosis. Sleep Med. Rev. *26*, 33–42.

Area-Gomez, E. (2014). Assessing the function of mitochondria-associated ER membranes. Methods Enzymol. *547*, 181–197.

Arvan, P., and Castle, D. (1998). Sorting and storage during secretory granule biogenesis: looking backward and looking forward. Biochem. J. *332*, 593–610.

Braak, H., Del Tredici, K., Rüb, U., de Vos, R.A.I., Jansen Steur, E.N.H., and Braak, E. (2003). Staging of brain pathology related to sporadic Parkinson's disease. Neurobiol. Aging *24*, 197–211.

Brogiolo, W., Stocker, H., Ikeya, T., Rintelen, F., Fernandez, R., and Hafen, E. (2001). An evolutionarily conserved function of the Drosophila insulin receptor and insulin-like peptides in growth control. Curr. Biol. *11*, 213–221.

Burman, J.L., Yu, S., Poole, A.C., Decal, R.B., and Pallanck, L. (2012). Analysis of neural subtypes reveals selective mitochondrial dysfunction in dopaminergic neurons from parkin mutants. Proc. Natl. Acad. Sci. USA *109*, 10438–10443.

Carvalho, M., Sampaio, J.L., Palm, W., Brankatschk, M., Eaton, S., and Shevchenko, A. (2012). Effects of diet and development on the Drosophila lipidome. Mol. Syst. Biol. *8*, 600.

Celardo, I., Costa, A.C., Lehmann, S., Jones, C., Wood, N., Mencacci, N.E., Mallucci, G.R., Loh, S.H.Y., and Martins, L.M. (2016). Mitofusin-mediated ER stress triggers neurodegeneration in pink1/parkin models of Parkinson's disease. Cell Death Dis. *7*, e2271.

Chiu, J.C., Low, K.H., Pike, D.H., Yildirim, E., and Edery, I. (2010). Assaying locomotor activity to study circadian rhythms and sleep parameters in Drosophila. J. Vis. Exp. *43*, e2157.

Clark, I.E., Dodson, M.W., Jiang, C., Cao, J.H., Huh, J.R., Seol, J.H., Yoo, S.J., Hay, B.A., and Guo, M. (2006). Drosophila pink1 is required for mitochondrial function and interacts genetically with parkin. Nature *441*, 1162–1166.

Crocker, A., Shahidullah, M., Levitan, I.B., and Sehgal, A. (2010). Identification of a neural circuit that underlies the effects of octopamine on sleep:wake behavior. Neuron *65*, 670–681.

Damiano, M., Gautier, C.A., Bulteau, A.L., Ferrando-Miguel, R., Gouarne, C., Paoli, M.G., Pruss, R., Auchère, F., L'Hermitte-Stead, C., Bouillaud, F., et al. (2014). Tissue- and cell-specific mitochondrial defect in Parkin-deficient mice. PLoS ONE *9*, e99898.

Dawson, T.M., and Dawson, V.L. (2010). The role of parkin in familial and sporadic Parkinson's disease. Mov. Disord. *25* (*Suppl 1*), S32–S39.

de Brito, O.M., and Scorrano, L. (2008). Mitofusin 2 tethers endoplasmic reticulum to mitochondria. Nature *456*, 605–610.

De Cock, V.C., Vidailhet, M., and Arnulf, I. (2008). Sleep disturbances in patients with parkinsonism. Nat. Clin. Pract. Neurol. *4*, 254–266.

de Lau, L.M., and Breteler, M.M. (2006). Epidemiology of Parkinson's disease. Lancet Neurol. *5*, 525–535.

De Pablo-Fernández, E., Breen, D.P., Bouloux, P.M., Barker, R.A., Foltynie, T., and Warner, T.T. (2017). Neuroendocrine abnormalities in Parkinson's disease. J. Neurol. Neurosurg. Psychiatry *88*, 176–185.

Deerinck, T.J., Bushong, E., Thor, A., and Ellisman, M. (2010). NCMIR methods for 3D EM: a new protocol for preparation of biological specimens for serial block face scanning electron microscopy. Nat. Center Microsc. Imag. Res. 6–8.

Depner, H., Lützkendorf, J., Babkir, H.A., Sigrist, S.J., and Holt, M.G. (2014). Differential centrifugation-based biochemical fractionation of the Drosophila adult CNS. Nat. Protoc. *9*, 2796–2808.

Erpapazoglou, Z., and Corti, O. (2015). The endoplasmic reticulum/mitochondria interface: a subcellular platform for the orchestration of the functions of the PINK1-Parkin pathway? Biochem. Soc. Trans. *43*, 297–301.

Esposito, G., Vos, M., Vilain, S., Swerts, J., De Sousa Valadas, J., Van Meensel, S., Schaap, O., and Verstreken, P. (2013). Aconitase causes iron toxicity in Drosophila pink1 mutants. PLoS Genet. *9*, e1003478.

Fifel, K., Piggins, H., and Deboer, T. (2016). Modeling sleep alterations in Parkinson's disease: How close are we to valid translational animal models? Sleep Med. Rev. *25*, 95–111.

Gautier, C.A., Kitada, T., and Shen, J. (2008). Loss of PINK1 causes mitochondrial functional defects and increased sensitivity to oxidative stress. Proc. Natl. Acad. Sci. USA *105*, 11364–11369.

Gautier, C.A., Erpapazoglou, Z., Mouton-Liger, F., Muriel, M.P., Cormier, F., Bigou, S., Duffaure, S., Girard, M., Foret, B., Iannielli, A., et al. (2016). The endoplasmic reticulum-mitochondria interface is perturbed in PARK2 knockout mice and patients with PARK2 mutations. Hum. Mol. Genet. *25*, 2972–2984.

Geisler, S., Holmström, K.M., Skujat, D., Fiesel, F.C., Rothfuss, O.C., Kahle, P.J., and Springer, W. (2010). PINK1/Parkin-mediated mitophagy is dependent on VDAC1 and p62/SQSTM1. Nat. Cell Biol. *12*, 119–131.

Graham, B.H., Li, Z., Alesii, E.P., Versteken, P., Lee, C., Wang, J., and Craigen, W.J. (2010). Neurologic dysfunction and male infertility in Drosophila porin mutants: a new model for mitochondrial dysfunction and disease. J. Biol. Chem. *285*, 11143–11153.

Greene, J.C., Whitworth, A.J., Kuo, I., Andrews, L.A., Feany, M.B., and Pallanck, L.J. (2003). Mitochondrial pathology and apoptotic muscle degeneration in Drosophila parkin mutants. Proc. Natl. Acad. Sci. USA *100*, 4078–4083.

Helfrich-Förster, C., and Homberg, U. (1993). Pigment-dispersing hormone-immunoreactive neurons in the nervous system of wild-type Drosophila melanogaster and of several mutants with altered circadian rhythmicity. J. Comp. Neurol. *337*, 177–190.

Helle, S.C.J., Kanfer, G., Kolar, K., Lang, A., Michel, A.H., and Kornmann, B. (2013). Organization and function of membrane contact sites. Biochim. Biophys. Acta *1833*, 2526–2541.

Hendricks, J.C., and Sehgal, A. (2004). Why a fly? Using Drosophila to understand the genetics of circadian rhythms and sleep. Sleep *27*, 334–342.

Hendricks, J.C., Finn, S.M., Panckeri, K.A., Chavkin, J., Williams, J.A., Sehgal, A., and Pack, A.I. (2000). Rest in Drosophila is a sleep-like state. Neuron *25*, 129–138.

Kasten, M., Kertelge, L., Brüggemann, N., van der Vegt, J., Schmidt, A., Tadic, V., Buhmann, C., Steinlechner, S., Behrens, M.I., Ramirez, A., et al. (2010). Nonmotor symptoms in genetic Parkinson disease. Arch. Neurol. *67*, 670–676.

Kim, H.Y., Huang, B.X., and Spector, A.A. (2014). Phosphatidylserine in the brain: metabolism and function. Prog. Lipid Res. *56*, 1–18.

Koh, K., Evans, J.M., Hendricks, J.C., and Sehgal, A. (2006). A Drosophila model for age-associated changes in sleep:wake cycles. Proc. Natl. Acad. Sci. USA *103*, 13843–13847.

Kornmann, B., Currie, E., Collins, S.R., Schuldiner, M., Nunnari, J., Weissman, J.S., and Walter, P. (2009). An ER-mitochondria tethering complex revealed by a synthetic biology screen. Science *325*, 477–481.

Kremer, J.R., Mastronarde, D.N., and McIntosh, J.R. (1996). Computer visualization of three-dimensional image data using IMOD. J. Struct. Biol. *116*, 71–76.

Kremer, A., Lippens, S., Bartunkova, S., Asselbergh, B., Blanpain, C., Fendrych, M., Goossens, A., Holt, M., Janssens, S., Krols, M., et al. (2015). Developing 3D SEM in a broad biological context. J. Microsc. *259*, 80–96.

Krols, M., van Isterdael, G., Asselbergh, B., Kremer, A., Lippens, S., Timmerman, V., and Janssens, S. (2016). Mitochondria-associated membranes as hubs for neurodegeneration. Acta Neuropathol. *131*, 505–523.

Kula-Eversole, E., Nagoshi, E., Shang, Y., Rodriguez, J., Allada, R., and Rosbash, M. (2010). Surprising gene expression patterns within and between PDF-containing circadian neurons in Drosophila. Proc. Natl. Acad. Sci. USA *107*, 13497–13502.

Kunst, M., Tso, M.C.F., Ghosh, D.D., Herzog, E.D., and Nitabach, M.N. (2015). Rhythmic control of activity and sleep by class B1 GPCRs. Crit. Rev. Biochem. Mol. Biol. *50*, 18–30.

Lee, H.M., and Koh, S.B. (2015). Many faces of Parkinson's disease: non-motor symptoms of Parkinson's disease. J. Mov. Disord. *8*, 92–97.

Lill, C., and Klein, C. (2015). The neurogenetics of Parkinson's disease and putative links to other neurodegenerative disorders. In Parkinson's Disease: Molecular Mechanisms Underlying Pathology, P. Verstreken, ed. (Academic), pp. 1–49.

Loh, Y.P. (1987). Peptide precursor processing enzymes within secretory vesicles. Ann. N Y Acad. Sci. *493*, 292–307.

Merkle, F.T., Maroof, A., Wataya, T., Sasai, Y., Studer, L., Eggan, K., and Schier, A.F. (2015). Generation of neuropeptidergic hypothalamic neurons from human pluripotent stem cells. Development *142*, 633–643.

Miśkiewicz, K., Schürmann, F.W., and Pyza, E. (2008). Circadian release of pigment-dispersing factor in the visual system of the housefly, Musca domestica. J. Comp. Neurol. *509*, 422–435.

Miskiewicz, K., Jose, L.E., Yeshaw, W.M., Valadas, J.S., Swerts, J., Munck, S., Feiguin, F., Dermaut, B., and Verstreken, P. (2014). HDAC6 is a Bruchpilot deacetylase that facilitates neurotransmitter release. Cell Rep. *8*, 94–102.

Morais, V.A., Verstreken, P., Roethig, A., Smet, J., Snellinx, A., Vanbrabant, M., Haddad, D., Frezza, C., Mandemakers, W., Vogt-Weisenhorn, D., et al. (2009). Parkinson's disease mutations in PINK1 result in decreased complex I activity and deficient synaptic function. EMBO Mol. Med. *1*, 99–111.

Morton, A.J. (2013). Circadian and sleep disorder in Huntington's disease. Exp. Neurol. *243*, 34–44.

Munhoz, R.P., Moro, A., Silveira-Moriyama, L., and Teive, H.A. (2015). Non-motor signs in Parkinson's disease: a review. Arq. Neuropsiquiatr. *73*, 454–462.

Paillusson, S., Stoica, R., Gomez-Suaga, P., Lau, D.H.W., Mueller, S., Miller, T., and Miller, C.C.J. (2016). There's something wrong with my MAM; the ER-mitochondria axis and neurodegenerative diseases. Trends Neurosci. *39*, 146–157.

Park, J., Lee, S.B., Lee, S., Kim, Y., Song, S., Kim, S., Bae, E., Kim, J., Shong, M., Kim, J.-M., and Chung, J. (2006). Mitochondrial dysfunction in Drosophila PINK1 mutants is complemented by parkin. Nature *441*, 1157–1161.

Park, J., Lee, G., and Chung, J. (2009). The PINK1-Parkin pathway is involved in the regulation of mitochondrial remodeling process. Biochem. Biophys. Res. Commun. *378*, 518–523.

Peeraully, T., Yong, M.H., Chokroverty, S., and Tan, E.K. (2012). Sleep and Parkinson's disease: a review of case-control polysomnography studies. Mov. Disord. *27*, 1729–1737.

Pesah, Y., Pham, T., Burgess, H., Middlebrooks, B., Verstreken, P., Zhou, Y., Harding, M., Bellen, H., and Mardon, G. (2004). Drosophila parkin mutants have decreased mass and cell size and increased sensitivity to oxygen radical stress. Development *131*, 2183–2194.

Peter-Derex, L., Yammine, P., Bastuji, H., and Croisile, B. (2015). Sleep and Alzheimer's disease. Sleep Med. Rev. *19*, 29–38.

Pickrell, A.M., and Youle, R.J. (2015). The roles of PINK1, parkin, and mitochondrial fidelity in Parkinson's disease. Neuron *85*, 257–273.

Politis, M., Wu, K., Molloy, S., G Bain, P., Chaudhuri, K.R., and Piccini, P. (2010). Parkinson's disease symptoms: the patient's perspective. Mov. Disord. *25*, 1646–1651.

Poole, A.C., Thomas, R.E., Yu, S., Vincow, E.S., and Pallanck, L. (2010). The mitochondrial fusion-promoting factor mitofusin is a substrate of the PINK1/parkin pathway. PLoS ONE *5*, e10054.

Poston, C.N., Krishnan, S.C., and Bazemore-Walker, C.R. (2013). In-depth proteomic analysis of mammalian mitochondria-associated membranes (MAM). J. Proteomics *79*, 219–230.

Prudent, J., Zunino, R., Sugiura, A., Mattie, S., Shore, G.C., and McBride, H.M. (2015). MAPL SUMOylation of Drp1 stabilizes an ER/mitochondrial platform required for cell death. Mol. Cell *59*, 941–955.

Rao, S., Lang, C., Levitan, E.S., and Deitcher, D.L. (2001). Visualization of neuropeptide expression, transport, and exocytosis in Drosophila melanogaster. J. Neurobiol. *49*, 159–172.

Renn, S.C., Park, J.H., Rosbash, M., Hall, J.C., and Taghert, P.H. (1999). A pdf neuropeptide gene mutation and ablation of PDF neurons each cause severe abnormalities of behavioral circadian rhythms in Drosophila. Cell *99*, 791–802.

Richter, C., Woods, I.G., and Schier, A.F. (2014). Neuropeptidergic control of sleep and wakefulness. Annu. Rev. Neurosci. *37*, 503–531.

Rulifson, E.J., Kim, S.K., and Nusse, R. (2002). Ablation of insulin-producing neurons in flies: growth and diabetic phenotypes. Science *296*, 1118–1120.

Schneider, C.A., Rasband, W.S., and Eliceiri, K.W. (2012). NIH Image to ImageJ: 25 years of image analysis. Nat. Methods *9*, 671–675.

Seibler, P., Graziotto, J., Jeong, H., Simunovic, F., Klein, C., and Krainc, D. (2011). Mitochondrial Parkin recruitment is impaired in neurons derived from mutant PINK1 induced pluripotent stem cells. J. Neurosci. *31*, 5970–5976.

Shivanandan, A., Radenovic, A., and Sbalzarini, I.F. (2013). MosaicIA: an ImageJ/Fiji plugin for spatial pattern and interaction analysis. BMC Bioinformatics *14*, 349.

Stichel, C.C., Augustin, M., Kühn, K., Zhu, X.R., Engels, P., Ullmer, C., and Lübbert, H. (2000). Parkin expression in the adult mouse brain. Eur. J. Neurosci. *12*, 4181–4194.

Stoleru, D., Peng, Y., Agosto, J., and Rosbash, M. (2004). Coupled oscillators control morning and evening locomotor behaviour of Drosophila. Nature *431*, 862–868.

Taymans, J.M., Van den Haute, C., and Baekelandt, V. (2006). Distribution of PINK1 and LRRK2 in rat and mouse brain. J. Neurochem. *98*, 951–961.

Valadas, J.S., Vos, M., and Verstreken, P. (2015). Therapeutic strategies in Parkinson's disease: what we have learned from animal models. Ann. N Y Acad. Sci. *1338*, 16–37.

Vos, M., Geens, A., Böhm, C., Deaulmerie, L., Swerts, J., Rossi, M., Craessaerts, K., Leites, E.P., Seibler, P., Rakovic, A., et al. (2017). Cardiolipin promotes electron transport between ubiquinone and complex I to rescue *PINK1* deficiency. J. Cell Biol. *216*, 695–708.

Vosko, A.M., Schroeder, A., Loh, D.H., and Colwell, C.S. (2007). Vasoactive intestinal peptide and the mammalian circadian system. Gen. Comp. Endocrinol. *152*, 165–175.

Wang, X., Winter, D., Ashrafi, G., Schlehe, J., Wong, Y.L., Selkoe, D., Rice, S., Steen, J., LaVoie, M.J., and Schwarz, T.L. (2011). PINK1 and Parkin target Miro for phosphorylation and degradation to arrest mitochondrial motility. Cell *147*, 893–906.

Wang, L., Meece, K., Williams, D.J., Lo, K.A., Zimmer, M., Heinrich, G., Martin Carli, J., Leduc, C.A., Sun, L., Zeltser, L.M., et al. (2015). Differentiation of hypothalamic-like neurons from human pluripotent stem cells. J. Clin. Invest. *125*, 796–808.

Westhead, E.W. (1987). Lipid composition and orientation in secretory vesicles. Ann. N Y Acad. Sci. *493*, 92–100.

Wong, M.Y., Zhou, C., Shakiryanova, D., Lloyd, T.E., Deitcher, D.L., and Levitan, E.S. (2012). Neuropeptide delivery to synapses by long-range vesicle circulation and sporadic capture. Cell *148*, 1029–1038.

Zanon, A., Kalvakuri, S., Rakovic, A., Foco, L., Guida, M., Schwienbacher, C., Serafin, A., Rudolph, F., Trilck, M., Grünewald, A., et al. (2017). SLP-2 interacts with Parkin in mitochondria and prevents mitochondrial dysfunction in Parkin-deficient human iPSC-derived neurons and Drosophila. Hum. Mol. Genet. *26*, 2412–2425.

STAR★METHODS

KEY RESOURCES TABLE

REAGENT or RESOURCE	SOURCE	IDENTIFIER
Antibodies		
anti-Pigment Dispersing Factor (PDF)	Developmental Studies Hybridoma Bank	Cat#PDF C7 RRID:AB_760350
anti-Insulin-like peptide 2 (dILP2)	Laboratory of Patrick Callaerts, KU Leuven	N/A
anti-Green fluorescent protein (GFP)	Invitrogen	Cat#A-11122 RRID:AB_221569
anti-Vasoactive Intestinal Peptide (VIP)	Abcam	Cat#ab8556 RRID:AB_306628
anti-Microtubule-associated protein 2 (MAP2)	Sigma-Aldrich	Cat#M1406 RRID:AB_477171
anti-β3tubulin	Biolegend	Cat#801201 RRID:AB_2313773
anti-Protein disulfide-isomerase (PDI)	Stressgen	Cat#SPA-891 RRID:AB_10615355
anti-TOM20	Santa Cruz Biotechnology	Cat#sc-11415 RRID:AB_2207533
anti-Calreticulin	Abcam	Cat#ab2907 RRID:AB_303402
anti-ATP synthase	Abcam	Cat#ab14730 RRID:AB_301438
anti-Discs large (DLG)	Developmental Studies Hybridoma Bank	Cat#4F3 RRID:AB_528203
Alexa Fluor 488 goat anti-mouse	Invitrogen	Cat#A-11029 RRID:AB_138404
Alexa Fluor 555 goat anti-rabbit	Invitrogen	Cat#A-21429 RRID:AB_141761
Alexa Fluor 555 goat anti-mouse	Invitrogen	Cat#A-21424 RRID:AB_141780
HRP conjugated anti-mouse	Jackson ImmunoResearch	Cat#115-035-166 RRID:AB_2338511
HRP conjugated anti-rabbit	Jackson ImmunoResearch	Cat#211-032-171 RRID:AB_2339149
Chemicals, Peptides, and Recombinant Proteins		
SAG	Millipore	Cat#566660
Purmorphamine	Millipore	Cat#540223
SB431542	Sigma-Aldrich	Cat#S4317
LDN-193189	Sigma-Aldrich	Cat#SML0559
BDNF	Preprotech	Cat#450-02
CNTF	Preprotech	Cat#450-13
GDNF	Preprotech	Cat#450-10
DAPT	Sigma-Aldrich	Cat#D5942
XAV939	Calbiochem	Cat#575545
BLOXALL	Vector laboratories	Cat#SP-6000
Diaminobenzidine	Sigma-Aldrich	Cat#D12384-5G
Osmium tetroxide	Polysciences	Cat#0972A-20
L-Aspartic acid	Sigma	Cat#A9256
Potassium hexacyanoferrate	Sigma	Cat#455989
Thiocarbohydrazide	Sigma	Cat#223220
Uranyl Acetate	Electron Microscopy Sciences	Cat#22400
Lead Nitrate	Merck	Cat#107398
Durcupan	Sigma-Aldrich	Cat#44611-14
L-α-phosphatidylserine (Brain, Porcine)	Avanti Polar Lipids	Cat#840032
L-α-phosphatidylcholine (Brain, Porcine)	Avanti Polar Lipids	Cat#840053
Critical Commercial Assays		
Drosophila activity monitor	Trikinetics	Cat#DAM2
Vectastain Elite ABC kit	Vector laboratories	Cat#PK-6102
ReliaPrep miRNA Cell and Tissue Miniprep System	Promega	Cat#Z6210

(*Continued on next page*)

Continued

REAGENT or RESOURCE	SOURCE	IDENTIFIER
SuperScript III First-Strand Synthesis System for RT-PCR	Thermofisher	Cat#18080051
LightCycler 480 SYBR Green I Master mix	Roche	Cat#4707516001
VIP ELISA kit	Aviva Systems Biology	Cat#OKEH00406
Experimental Models: Cell Lines		
Human IPSC: control L4993	Zanon et al., 2017	N/A
Human IPSC: control L5991	Zanon et al., 2017	N/A
Human IPSC: parkin mutant L3048	Zanon et al., 2017	N/A
Human IPSC: parkin mutant L5415	Zanon et al., 2017	N/A
Human IPSC: pink1 mutant L2124	Seibler et al., 2011	N/A
Human IPSC: pink1 mutant L2126	Seibler et al., 2011	N/A
Experimental Models: Organisms/Strains		
D. melanogaster: w^{1118}	BDSC	RRID:BDSC_3605; Fly base: FBal0018186
D. melanogaster: $parkin^{1}$	BDSC	RRID:BDSC_34747; Fly base: FBst0034747
D. melanogaster: $parkin^{\Delta 21}$	BDSC	RRID:BDSC_51652; Fly base: FBst0051652
D. melanogaster: $parkin^{25}$	Greene et al., 2003	Fly base: FBal0146938
D. melanogaster: $pink1^{B9}$	BDSC	RRID:BDSC_34749; Fly base: FBst0034749
D. melanogaster: pink1-myc	Clark et al., 2006	Fly base: FBal0196296
D. melanogaster: parkin rescue (dpkR)	Pesah et al., 2004	Fly base: FBal0158834
D. melanogaster: parkin rescue STOP (dpkSR)	Pesah et al., 2004	Fly base: FBal0158826
D. melanogaster: Tubulin-Gal4	BDSC	RRID:BDSC_30029; Fly base: FBst0030029
D. melanogaster: Elav-Gal4	BDSC	RRID:BDSC_8765; Fly base: FBst0008765
D. melanogaster: PDF-Gal4	BDSC	RRID:BDSC_6900; Fly base: FBst0006900
D. melanogaster: sNPF-Gal4	BDSC	RRID:BDSC_51991; Fly base: FBst0051991
D. melanogaster: Ilp2-Gal4	BDSC	RRID:BDSC_37516; Fly base: FBst0037516
D. melanogaster: c929-Gal4	BDSC	RRID:BDSC_25373; Fly base: FBst0025373
D. melanogaster: DH31-Gal4	BDSC	RRID:BDSC_51988; Fly base: FBst0051988
D. melanogaster: c253-Gal4	BDSC	RRID:BDSC_6980; Fly base: FBst0006980
D. melanogaster: c309-Gal4	BDSC	RRID:BDSC_6906; Fly base: FBst0006906
D. melanogaster: c305-Gal4	BDSC	RRID:BDSC_30829; Fly base: FBst0030829
D. melanogaster: 50y-Gal4	BDSC	RRID:BDSC_30820; Fly base: FBst0030820
D. melanogaster: c767-Gal4	BDSC	RRID:BDSC_30848; Fly base: FBst0030848
D. melanogaster: c316-Gal4	BDSC	RRID:BDSC_30830; Fly base: FBst0030830
D. melanogaster: c232-Gal4	BDSC	RRID:BDSC_30828; Fly base: FBst0030828
D. melanogaster: C5-Gal4	BDSC	RRID:BDSC_30839; Fly base: FBst0030839
D. melanogaster: Tdc2-Gal4	BDSC	RRID:BDSC_9313; Fly base: FBst0009313
D. melanogaster: ple-Gal4	BDSC	RRID:BDSC_8848; Fly base: FBst0008848
D. melanogaster: PDF-Gal80	Laboratory of Sha Liu, KU Leuven/VIB	Fly base: FBti0074329
D. melanogaster: UAS-$parkin^{RNAi}$ (KK107919)	VDRC	# 104363; Fly base: FBst0476221
D. melanogaster: UAS-$parkin^{RNAi}$ #2 (JF01200)	BDSC	RRID:BDSC_31259; Fly base: FBst0031259
D. melanogaster: UAS-$pink1^{RNAi}$ (JF01672)	BDSC	RRID:BDSC_31170; Fly base: FBst0031170
D. melanogaster: UAS-$pink1^{RNAi}$ #2 (HMC04160)	BDSC	RRID:BDSC_55886; Fly base: FBst0055886
D. melanogaster: UAS-$control^{RNAi}$(for BDSC Trip lines)	BDSC	RRID:BDSC_31603; Fly base: FBst0031603
D. melanogaster: UAS-$control^{RNAi}$ (for VDRC KK lines)	VDRC	# 60100
D. melanogaster: UAS-hid	BDSC	RRID:BDSC_65403; Fly base: FBst0065403
D. melanogaster: UAS-ricin	BDSC	RRID:BDSC_28999; Fly base: FBst0028999
D. melanogaster: UAS-preproANF-GFP	BDSC	RRID:BDSC_7001; Fly base: FBst0007001

(*Continued on next page*)

Continued

REAGENT or RESOURCE	SOURCE	IDENTIFIER
D. melanogaster: UAS-Syt-GFP	BDSC	RRID:BDSC_6925; Fly base: FBst0006925
D. melanogaster: UAS-dIlp2-GFP	Wong et al., 2012	Fly base: FBrf0217647
D. melanogaster: UAS-mitoGFP	BDSC	RRID:BDSC_8442; Fly base: FBst0008442
D. melanogaster: UAS-mitotdtomato	DGRC	RRID:DGGR_117016
D. melanogaster: UAS-KDELGFP	BDSC	RRID:BDSC_9898; Fly base: FBst0009898
D. melanogaster: UAS-MARF	Park et al., 2009	Fly base: FBal0230288
D. melanogaster: UAS-Porin	Graham et al., 2010	Fly base: FBal0246185
D. melanogaster: UAS-ChiMERA	This paper	n/a
D. melanogaster: UAS-MARF^{RNAi}	VDRC	# 105261; Fly base: FBst0477089
D. melanogaster: UAS-GFP	BDSC	RRID:BDSC_5431; Fly base: FBst0005431
D. melanogaster: UAS-PtdSer synthase^{RNAi}	VDRC	# 105470; Fly base: FBst0477297
Software and Algorithms		
ImageJ 1.51	National Institute of Health	https://imagej.nih.gov/ij/
Prism 7	GraphPad Software	https://www.graphpad.com/scientific-software/prism/
Inkscape 0.92.2	Inkscape's Contributors	https://inkscape.org/en/release/0.92.2/
IMOD 4.9	Mastronarde Group | University of Colorado	http://bio3d.colorado.edu/imod/
NIS-Elements 4.13	Nikon	https://www.nikoninstruments.com/
FaasX 1.21	François Rouyer lab	http://neuro-psi.cnrs.fr/IMG/FaasX/FaasX_Kit.zip
Microsoft Excel 2016	Microsoft Corporation	https://products.office.com/en-US/

CONTACT FOR REAGENT AND RESOURCE SHARING

Further information and requests for resources and reagents should be directed to the Lead Contact Patrik Verstreken (patrik.verstreken@kuleuven.vib.be). Human IPSC were used in accordance with an MTA with the University of Lübeck.

EXPERIMENTAL MODEL AND SUBJECT DETAILS

Fly stocks and maintenance

Drosophila melanogaster fly stocks were handled using standard protocols, kept in a 12 hr light/dark cycle and fed a standard *Drosophila* diet consisting of cornmeal, agar, yeast, sucrose, and dextrose. All experimental crosses were kept at 25°C. Mutant and transgenic stocks were obtained from the Bloomington *Drosophila* Stock Center (BDSC), Kyoto Stock Center (DGRC), the Vienna *Drosophila* RNAi stock center (VDRC) or were gifts (see Key Resources Table for details). *parkin*^{1}, *parkin*$^{\Delta 21}$, *parkin*^{25} are null mutants of *parkin*, and *pink1*^{B9} is a null mutant of *pink1*. Rescue flies express a genomic fragment containing *parkin* or *pink1* (Clark et al., 2006; Pesah et al., 2004). Rescue STOP flies express a genomic fragment containing *parkin* but with a premature STOP codon, preventing Parkin expression (Pesah et al., 2004). *w*^{1118} was used as control for *parkin* and *pink1* mutants. Flies expressing an RNAi against luciferase (BDSC 31603) were used as control for all TRIP RNAi lines and flies with an empty landing site (VDRC 60100) were used as control for the KK RNAi lines.

The UAS-ChiMERA construct (Kornmann et al., 2009) was generated using standard cloning procedures (using EcoRI and XhoI to integrate the ChiMERA in a pUAS vector). After confirming the sequence of the plasmid, germline transformation was achieved by injection of embryos at BestGene (USA) using the VK00037 landing site.

iPSC maintenance and differentiation

iPSC from 2 *parkin* patients with gene deletions and point mutations (lines L3048, male; and L5415, female), 2 *PINK1* patients with a premature STOP codon (lines L2124 and L2126, both females) as well as 2 matched controls (lines L4993 and L5991, both females, Figure S4B, Seibler et al., 2011; Zanon et al., 2017) were differentiated into hypothalamic neurons according to a protocol described before (Merkle et al., 2015). Briefly, cells were maintained in matrigel coated plates with mTeSR1 (Stem Cell Technologies) and medium changes were performed every two days. For hypothalamic neuron differentiation, the supplements and media used are described in Figure S4A. After 14 days, cells were trypsinized and replated with maturation medium. At day 30, coverslips

with differentiated neurons were placed over cultured rat glia for 10 days and then prepared for immunolabeling or neuropeptide release experiments.

METHOD DETAILS

Fly activity assay

Male flies were selected from each group to be analyzed in the *Drosophila* Activity Monitor (DAM, from Trikinetics) in a 25°C incubator. 2- to 5-day-old male flies are individually introduced in DAM glass tubes (Chiu et al., 2010). After 24 hr of habituation, fly activity was recorded for at least 3 consecutive days. The number of assays is indicated in the figure legends. Morning anticipation is defined as the ratio between the increase of the transitions in 3 hr that precede the light change (transitions $_{3\rightarrow0}$ subtracted the basal activity, transitions $_{6\rightarrow3}$) to the transitions on the 6 hr preceding the lights-on event (transitions $_{3\rightarrow0}$ + transitions $_{6\rightarrow3}$). The morning anticipation score of animals that do not increase their activity in the 3 hr before the lights-on event is represented as zero, while the score for animals that increase their activity in the last 3 hr of the dark period is a positive value.

$$morning\ anticipation(\%) = \frac{transitions_{3\rightarrow0} - transitions_{6\rightarrow3}}{transitions_{3\rightarrow0} + transitions_{6\rightarrow3}} \times 100.$$

The evening anticipation score was calculated with the same formula but taking as reference the lights-off event. Brief awakenings are periods of a maximum of 5 min with less than 4 transitions between 2 sleep events (Koh et al., 2006). Basal motor performance (waking activity) was evaluated by the number of transitions in an active minute (Chiu et al., 2010). For dark/dark experiments, flies were habituated for 7 days in the 12 hr light/dark condition before the lights are turned off and activity was recorded for at least 4 days. Quantification of the circadian period, the percentage of rhythmic flies and the power of the circadian cycle are presented (Chiu et al., 2010). Data analysis was performed with a custom-made Microsoft Excel file and FaasX.

Drosophila neuropeptide distribution and mitochondria morphology

One hour before the lights-on event (*Zeitgeber* Time 23), fly brains were dissected in cold PBS, fixed in FA 3.7%, washed with PBS (0.05%Triton X-100), blocked with NGS 10% in PBS (0.05%Triton X-100) for 1 hr, incubated overnight at 4°C with antibodies for PDF (PDF C7 Hybridoma Bank 1:50) or dIlp2 (gift from Patrick Callaerts, KU Leuven, 1:500), washed with PBS (0.05%Triton X-100), incubated with secondary anti-mouse or anti-rabbit alexa antibodies for 1 hr (1:500), washed with PBS (0.05%Triton X-100), and mounted (in Vectashield) on a microscope slide. Confocal stacks of LNv and IPC neurons were acquired with the Nikon A1R confocal microscope through a 20x NA 0.75, 40X NA1.15 or 60X NA1.2 water immersion lens and signal was quantified in ImageJ (Schneider et al., 2012). Images were summed to quantify the total neuropeptide signal in the neuron.

Staining in human differentiated neurons

After 40 days of differentiation, cells were fixed in 4% PFA for 30 min, washed with PBS, blocked with 5% NGS in PBS with 0.3% Triton X-100, incubated overnight at 4°C with antibodies for Vasoactive Intestinal Peptide (VIP, Abcam ab8556 1:100), Microtubule-associated protein 2 (MAP2, sigma M1406 1:1000), β3tubulin (Biolegend 8020001 1:1000), TOM20 (sc-11415 1:500) or Protein disulfide-isomerase (PDI, Stressgen SPA-891 1:500), washed with PBS, incubated with secondary anti-mouse or anti-rabbit alexa antibodies for 1 hr (1:500), washed with PBS, and mounted on a microscope slide with ProLong Diamond Antifade Mountant with DAPI (Thermo Fisher). Images were acquired with the Nikon A1R confocal microscope through a 40X NA1.15 or 60X NA1.2 water immersion lens and signal was quantified with ImageJ (Schneider et al., 2012) and the MOSAIC plugin (Shivanandan et al., 2013).

Neuropeptide secretion

Medium from differentiated neurons at day 40 was changed and collected after 20 min (basal release of neuropeptides). Cells were then incubated for 20 min with Maturation medium (control) or Maturation medium with 60 mM KCl. Medium was again collected and frozen until analysis (Wang et al., 2015). VIP levels were measured with VIP ELISA Kit (Aviva Systems Biology OKEH00406) and results are reported as the ratio between the induced release (with KCl) and the unstimulated release (control).

ER-mitochondria distance in flies

One hour before the lights-on event (*Zeitgeber* Time 23), fly brains were dissected in cold PBS, fixed in FA 3.7%, washed 3 times with PBS (0.05%Triton X-100) and mounted (in Vectashield) on a microscope slide. Images were acquired with the Nikon A1R confocal microscope through a 60X NA1.2 water immersion lens and quantified with ImageJ using the MOSAIC plugin (Shivanandan et al., 2013). Briefly, images of ER and mitochondria were thresholded with ImageJ, such that all ER and mitochondria positive pixels are each visible as an area. These areas are transformed into perimeters (removing the inside of the shape). Using the Mosaic plugin for ImageJ, we computed the minimal distance between each pixel of the ER perimeter to the perimeter of the mitochondria. We then calculated the sum of all the frequencies with a distance below 1 pixel (Figures 6B, 6D, 6G) as a measurement of the proximity of ER and mitochondria.

Western blotting

Samples were homogenized in RIPA buffer with protease inhibitors. Protein concentration was determined using the Quick Start Bradford Dye Reagent (BioRad) and measured as absorbance at 600 nm in a GloMax Multi Detection Plate Reader (Promega). After denaturation, samples separated by SDS-PAGE, transferred to a nitrocellulose membrane (Miskiewicz et al., 2014) and probed against GFP (Invitrogen A-11122 1:2000), Calreticulin (abcam ab2907 1:1000), ATP synthase (abcam ab147301:1000) or Discs large (DLG, DSHB 4F3 1:1000). The ECL system (Perkin Elmer) was used for detection and chemiluminescence was imaged using LAS-3000 (Fuji Film). The intensity of bands was quantified with ImageJ (Schneider et al., 2012).

Electron microscopy

Dissected fly brains were fixed in 2% formaldehyde + 2% glutaraldehyde, embedded in agarose and sectioned in 70 μm thick slices. After permeabilization (PBS Triton X-100 0.02%), inhibition of endogenous Peroxidase (BLOXALL) and blocking (PBS Triton 0.02%, BSA 0.25%, NGS 10%), slices were labeled with PDF antibody (PDF C7 Hybridoma Bank 1:50, in BSA 0.25%) and probed with Vectastain Elite ABC kit followed by HRP oxidation of DAB 0.025% (Miśkiewicz et al., 2008). Samples were treated for EM imaging: post-fixation (1% FA/1% GA), incubated with 1.5% ferrocyanide and OsO_4 4% and then Thiocarbohydrazide 1%. After incubation with OsO_4 1%, slices were incubated in Uranyl acetate 1% and then Walton Lead Aspartate. Slices were dehydrated with a series of ethanol solutions and embedded in durcupan resin (Deerinck et al., 2010). PDF labeled cells in the fly brain were approached using a serial Block-Face scanning electron microscope (Zeiss Merlin). When the first images of these cells were acquired, the sample was moved to a Focused Ion Beam scanning electron microscope (FIB-SEM) (Zeiss Auriga) where high resolution images were acquired (Figures S5A and S5B) (Kremer et al., 2015). Image modeling and quantification was performed with IMOD (Kremer et al., 1996) and ImageJ software (Schneider et al., 2012). TEM images were obtained from 50 nm sections imaged on a JEM2100 (JEOL) microscope (Miskiewicz et al., 2014).

Quantitative real-time PCR

Total RNA was extracted from 9-10 fly brains using the ReliaPrep miRNA Cell and Tissue Miniprep System (Promega). The manufacturer's protocol was followed including a DNaseI treatment to prevent DNA contamination. Subsequently, cDNA was amplified from 1 μg of RNA using the SuperScript III First-Strand Synthesis System for RT-PCR (Life Technologies) using a mix of oligo(dt) primers and random hexamer primers. A mock control without reverse transcriptase was included for all samples. Next, 4.5 μL of 25 ng/μL cDNA, mock or water (no template control) were loaded together with 0.5 μM of the forward and reverse primers for PDF, Parkin, Pink1, MARF or PS synthase (PSs) and the LightCycler 480 SYBR Green I Master mix (Roche). Subsequently, the LightCycler 480 was used for analysis (Roche). Primers are listed below. The ribosomal protein RP49 was used as house-keeping gene to normalize the data for loading differences. The fold change of mRNA expression was determined for each gene using the Δ-Δ-CT method, where the expression of the genes was compared to the control sample.

PDF_Fw GCTCGCTACACGTACCTTGT
PDF_Rv GATAGCGACAGAGAGTGGCC
dPark_Fw GGAGCGTCTGAATATAACCGATG
dPark_Rv GGATCACGATGGACAGTAAAGG
dPink1_Fw AAGCGAGGCTTTCCCCTAC
dPink1_Rv GCACTACATTGACCACCGATTT
MARF_Fw GAGACGACCACCTTTATCAACG
MARF_Rv GCCACCTTCATGTGATCCCG
PSs_Fw TTCTACAAGCCACACACCATC
PSs_Rv CGTTTCTGACGAACGCAAAGTA
RP-49_F ATCGGTTACGGATCGAACAA
RP-49_R GACAATCTCCTTGCGCTTCT

Lipid measurement in ER and mitochondrial fractions

Flies were snap frozen, heads were isolated and homogenized in buffer (Sucrose 320 mM, HEPES 4 mM, $MgCl_2$ 1.5 mM, pH 7.4, with protease inhibitors) (Depner et al., 2014). Homogenate (H) was spun at 1000 *g* for 10 min. The supernatant (S1) was collected and spun at 13000 *g* for 15 min followed by a washing step of the pellet containing the mitochondria (P2) with 1 mL of buffer. The supernatant (S2) was collected and spun at 124000 *g* for 1 hr to obtain a pellet enriched with ER membrane (P3). Mass spectrometry–based lipid analysis of H, P2 and P3 was performed at Lipotype GmbH as previously described (Vos et al., 2017). Ratios between the lipid amount in the ER (P3) to the amount in mitochondria (P2) are shown.

Lipid supplemented food experiment

Food supplemented with 150 μM PtdSer or 300 μM PtdCho (1500x the amount of these lipids in the fly food (Carvalho et al., 2012)) was prepared from the lipid stock in chloroform (25 mg/mL). The same volume of Chloroform was added in the control experiment. 1- to 3-day-old flies were used at the beginning of each experiment.

QUANTIFICATION AND STATISTICAL ANALYSIS

Statistical Analysis

Statistical analyses were performed using GraphPad Prism 7.0 software. The criteria for significance is: ns (not significant) $p > 0.05$, $^{*}p < 0.05$, $^{**}p < 0.01$, $^{***}p < 0.001$. Significant differences between 2 groups were analyzed using a two-tailed Mann-Whitney test. For more than 2 groups, a one-way ANOVA (with Bonferroni's post hoc correction for multiple comparisons) was used. For the lipid supplementation analysis, a two-way ANOVA (with Tukey post hoc correction for multiple comparisons) was used. The graph representation and error bars are defined in each legend, together with the definition of n and which statistical test was performed. Error bars show standard error of the mean (SEM), as indicated in the figure legend. Sample size was chosen according to that used for similar experiments in the literature.

Neuron, Volume *98*

Supplemental Information

ER Lipid Defects in Neuropeptidergic Neurons Impair Sleep Patterns in Parkinson's Disease

Jorge S. Valadas, Giovanni Esposito, Dirk Vandekerkhove, Katarzyna Miskiewicz, Liesbeth Deaulmerie, Susanna Raitano, Philip Seibler, Christine Klein, and Patrik Verstreken

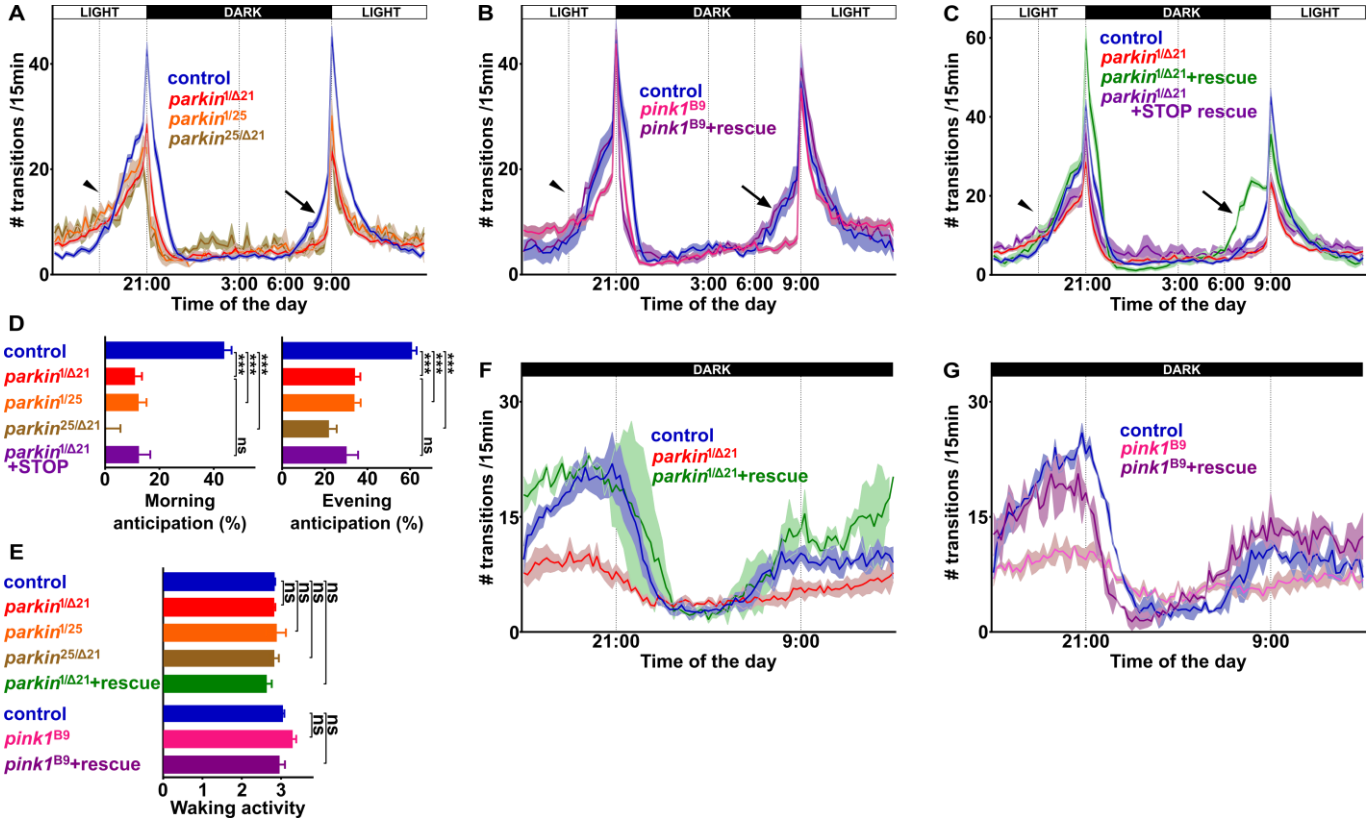

Figure S1. Defects in the circadian rhythms of parkin and pink1 mutant fruit flies. Related to Figure 1.

(A-D) 24 h average activity plotted as the number of infrared beam breaks measured per 15 min of control flies and flies carrying different null mutant alleles of *parkin* (**A**) and *pink1* (**B**) and of mutant flies with a wild type or mutated (STOP rescue) genomic rescue construct (**B**, **C**) as well as quantification of morning (arrows) and evening (arrowheads) anticipation (**D**). n=3-22 assays with 25 flies each in A and D; 3-6 assays with 25 flies each in B and n=3-7 assays with 25 flies each in C and D. ns: not significant, ***p<0.001 by Bonferroni's test following one-way ANOVA. Data are represented as mean ± SEM.

(E) The flies used in this study do not display obvious motor impairments that would confound the analyses of circadian rhythmicity and sleep. Waking activity is defined as the number of transitions between the two sides of the tube normalized to the number of active minutes. n=3-22 assays with 25 flies each. ns: not significant by Bonferroni's test following one-way ANOVA. Data are represented as mean ± SEM.

(F-G) 24 h average activity plotted as the number of infrared beam breaks measured per 15 min of flies of the genotypes used in A-D, now first trained for 7 d in 12 h light dark cycles and then monitored in dark conditions. Quantification in Figure 1 D-F showing that *parkin* and *pink1* mutants show significant circadian defects, including a decrease in the number of rhythmic flies and in the circadian power.

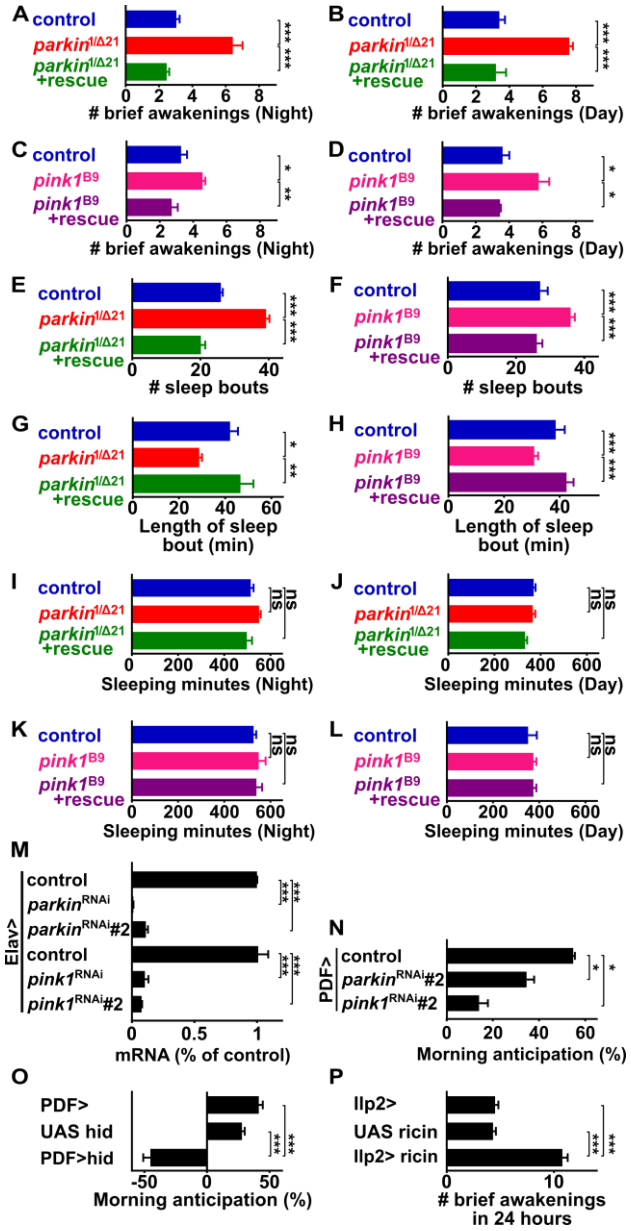

Figure S2. Quantification of sleep parameters in *parkin* and *pink1* mutants. Related to Figure 1 and Figure 2.

(A-L) Quantification of circadian and sleep parameters: the number of nighttime (**A**, **C**) and daytime (**B**, **D**) brief awakenings, the number of sleep bouts (periods of more than 5 min without activity, **E**, **F**), the length of sleep (the average length of the sleep bouts, **G**, **H**) and the sleeping minutes (total amount of sleep bout minutes in a 24 h period) during the night (**I**, **K**) and during the day (**J**,**L**) in controls, *parkin* and *pink1* mutants (with or without a genomic rescue construct). n=5-9 assays with >25 flies per assay in A-D; n=4-8 assays with >25 flies per assay in E-H; n=4-8 assays with > 25 flies per assay in I-L. ns: not significant, *p<0.05, **p<0.01, ***p<0.001 by Bonferroni's test following one-way ANOVA. Data are represented as mean ± SEM.

(M) Quantitative RT-PCR of *Parkin* and *Pink1* RNA in fly brains that express RNAi to *parkin* and *pink1* respectively under control of Elav-Gal4. Two different RNAi constructs per gene were used: Parkin^{RNAi} (KK107919) and Parkin^{RNAi}#2 (JF01200) and Pink1^{RNAi} (JF01672) and Pink1^{RNAi}#2 (HMC04160)). n=3 independent assays. ***p<0.001 by Bonferroni's test following one-way ANOVA. Data are represented as mean ± SEM.

(N) Quantification of morning anticipation in animals that express Parkin^{RNAi}#2 or Pink1^{RNAi}#2 in LNv. n=3 assays with > 25 flies per assay. *p<0.05 by Bonferroni's test following one-way ANOVA. Data are represented as mean ± SEM.

(O, P) Quantification of morning anticipation (**O**) or brief awakenings (**P**) in animals that express the pro-apoptotic factor hid in LNv neurons (O, PDF-Gal4) or the toxin ricin in IPC (P, Ilp2-Gal4) causing the ablation of the LNv or IPC neurons respectively. n=30-33 flies in O and n=25-31 flies in P. ***p<0.001 by Bonferroni's test following one-way ANOVA. Data are represented as mean ± SEM.

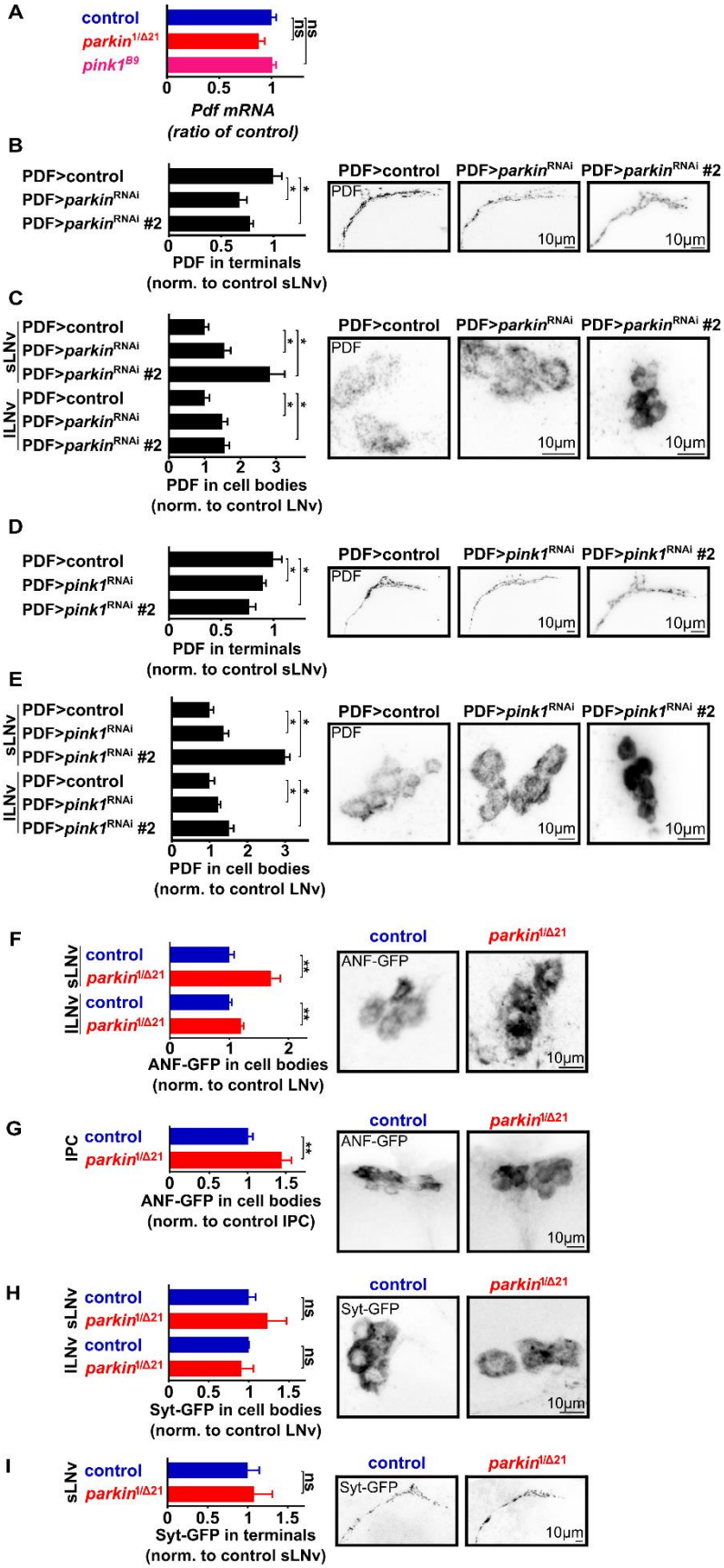

Figure S3. Parkin or Pink1 are required in a cell autonomous manner for neuropeptide localization to terminals. Related to Figure 3.

(A) Quantitative RT-PCR of *Pdf* RNA in fly heads of *parkin* and *pink1* null mutants. n=3 independent assays. ns: not significant by Bonferroni's test following one-way ANOVA. Data are represented as mean ± SEM.

(B-E) Quantification of labeling intensity and images of anti-PDF labeled LNv terminals (**B**, **D**) and cell bodies (**C**, **E**) of animals expressing RNAi to Parkin (Parkin^{RNAi} or Parkin^{RNAi}#2, B, C) or to Pink1 (Pink1^{RNAi} or Pink1^{RNAi}#2, D, E) in LNv neurons

(PDF-Gal4). Animals were dissected at *Zeitgeber* time 23. n=3-17 animals in B and C, n=3-41 animals in D and E. *p<0.05 by Bonferroni's test following one-way ANOVA. Data are represented as mean ± SEM.

(F-I) Quantification of fluorescence intensity and images of ANF-GFP (**F, G**) and Syt-GFP (**H, I**) in cell bodies (F-H) or neuronal terminals (I) of these tools expressed in LNv neurons (PDF-Gal4, F, H-I) or IPC neurons (dIlp2-Gal4, G) in controls and *parkin* mutants. n=44-45 for F; n= 22-29 for G ; n=24-36 for H and n=9-12 for I. ns: not significant, **p<0.01 by Bonferroni's test following one-way ANOVA in F and H. ns: not significant; **p<0.01 by Mann-Whitney test in G and I. Data are represented as mean ± SEM.

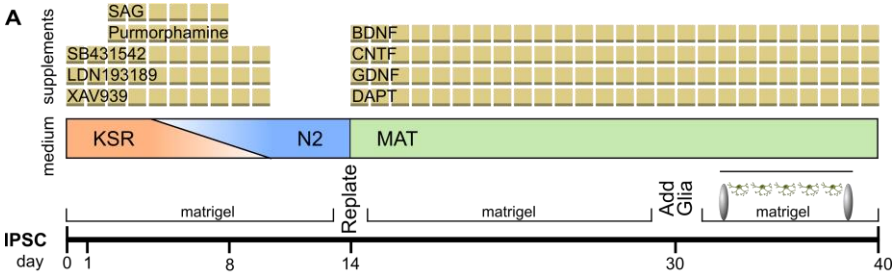

B

	ID	Sex	Age at biopsy (yr)	Age at onset (yr)	Mutation	Zygosity	Clinical status	Sleep symptoms
***parkin* mutation carriers**	L3048	M	57	15	delEx4; c.924C>T	compound heterozygous	affected	Yes
	L5415	F	35	n/a	c.823C>T; c.1054T>C	compound heterozygous	affected	Yes
***pink1* mutation carriers**	L2124	F	61	53	c.1366C>T	homozygous	affected	Yes
	L2126	F	72	47	c.1366C>T	homozygous	affected	Yes
controls	L4993	F	63	-	-	-	unaffected	No
	L5991	F	67	-	-	-	unaffected	No

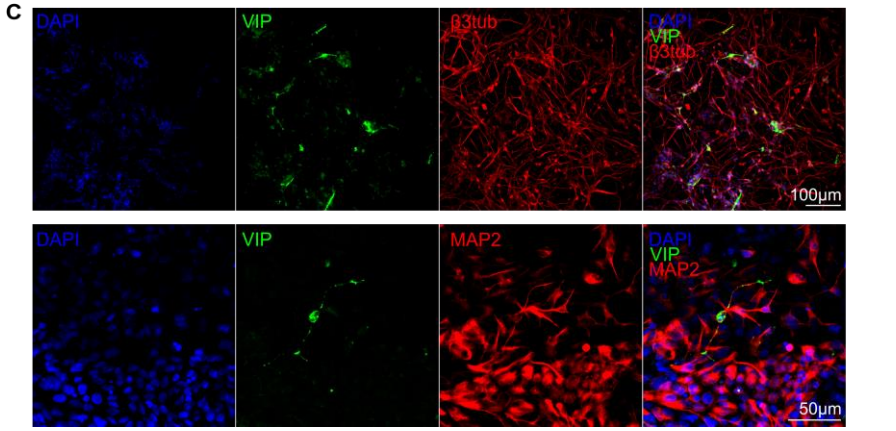

Figure S4. Differentiated human hypothalamic neurons from iPSC express neuropeptides and mature neuronal markers. Related to Figure 4.

(A) Differentiation protocol for hypothalamic neurons from iPSC (adapted from Merkle et al., 2015).

(B) Genotypic and phenotypic information of the Parkinson's disease patients and control individuals from which iPSC were generated and used in this study.

(C) Images of cells differentiated from iPSC using the protocol indicated in (A) and labelled after 40 days of differentiation with anti-VIP (a neuropeptide homologous to fly PDF, green) and markers of neuron maturation (anti-β3tubulin and anti-MAP2, in red). The nuclei are labeled with DAPI (blue).

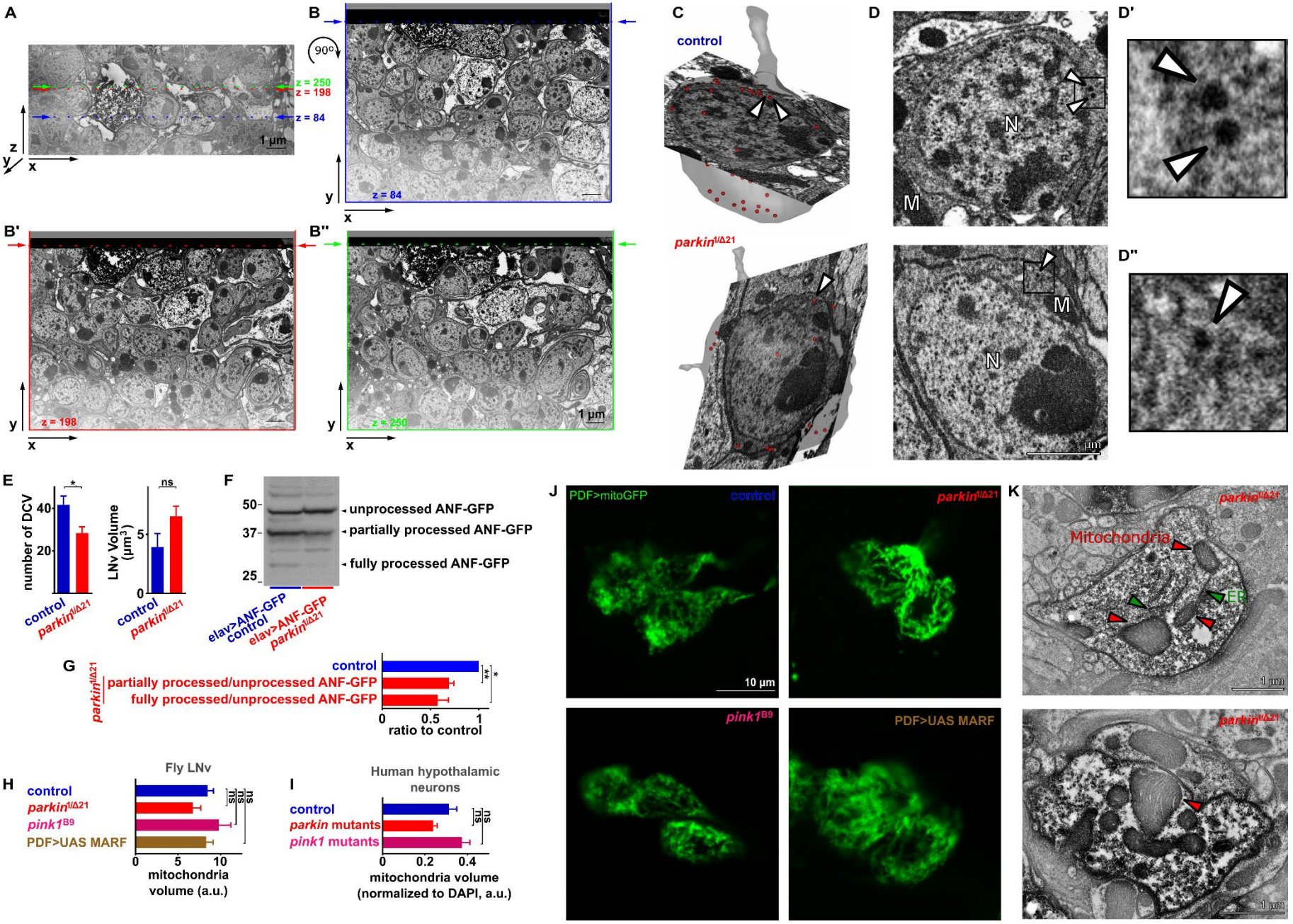
A
B
B'
B''
z = 250
z = 198
z = 84
1 µm
90°
C
control
parkin1/Δ21
D
D'
D''
N
M
E
number of DCV
LNv Volume (µm3)
control
parkin1/Δ21
ns
F
50
37
25
unprocessed ANF-GFP
partially processed ANF-GFP
fully processed ANF-GFP
elav>ANF-GFP control
elav>ANF-GFP parkin1/Δ21
G
parkin1/Δ21
partially processed/unprocessed ANF-GFP
fully processed/unprocessed ANF-GFP
ratio to control
H
Fly LNv
control
parkin1/Δ21
pink1B9
PDF>UAS MARF
mitochondria volume (a.u.)
I
Human hypothalamic neurons
control
parkin mutants
pink1 mutants
mitochondria volume (normalized to DAPI, a.u.)
J
PDF>mitoGFP
control
parkin1/Δ21
pink1B9
PDF>UAS MARF
10 µm
K
Mitochondria
ER

Figure S5. Normal mitochondrial morphology and Dense core vesicle defects in Parkinson's disease mutants. Related to Figure 5.

(A) Block-face scanning electron microscopy image of cells labeled using anti-PDF conjugated with HRP. Cartesian coordinates are marked with arrows and dashed lines.

(B-B'') Focused ion beam scanning electron microscopy images at different Z planes indicated in (A): B) z=84 µm in blue, B') z=198 µm in red and B'') z=250 µm in green. The top of each plane (marked with a dashed line) corresponds to the line indicated in (A).

(C-D'') Models of LNv cell bodies reconstructed from focused ion beam SEM images from control and *parkin* mutants. One section of the stack is shown and DCVs are indicated by arrows. This same section is also shown in D; DCV, white arrows, 50 to 70 nm in diameter; mitochondria (M) and nucleus (N). D' and D'' are magnifications for the areas indicated in D.

(E) Quantification of the amount of DCV in the LNv cell bodies and the LNv cell body volume in control and *parkin* mutants. n=6-7 reconstructions, from 4 control brains and 4 *parkin* mutant brains. ns: not significant, **p*<0.05 by Mann-Whitney test. Data are represented as mean ± SEM.

(F-G) Western blot of adult fly heads expressing ANF-GFP in neurons (Elav-Gal4) in control and *parkin* mutant flies probed with anti-GFP. The bands for unprocessed, partially processed and fully processed ANF-GFP are indicated (F) and the quantification of the intensity of each band normalized to total neuropeptide (G). n=3 independent experiments. *p<0.05; **p<0.01 by Bonferroni's test following one-way ANOVA. Data are represented as mean ± SEM.

(H-I) Quantification of mitochondrial volume from images of mito-GFP labeling expressed in fly LNv (**H**) or in induced human hypothalamic neurons (**I**). ns: not significant by Bonferroni's test following one-way ANOVA. Data are represented as mean ± SEM.

(J) The morphology of LNv mitochondria is not altered by mutations in *parkin* or *pink1* or with MARF overexpression in LNvs (images obtained by mitoGFP expression in the LNv neurons).

(K) Transmission electron micrograph of *parkin* mutant LNv cell bodies labeled by anti-PDF coupled to HRP to reveal the structure and integrity of the mitochondria and cristae. Mitochondria: red arrowheads; ER: green arrowheads.

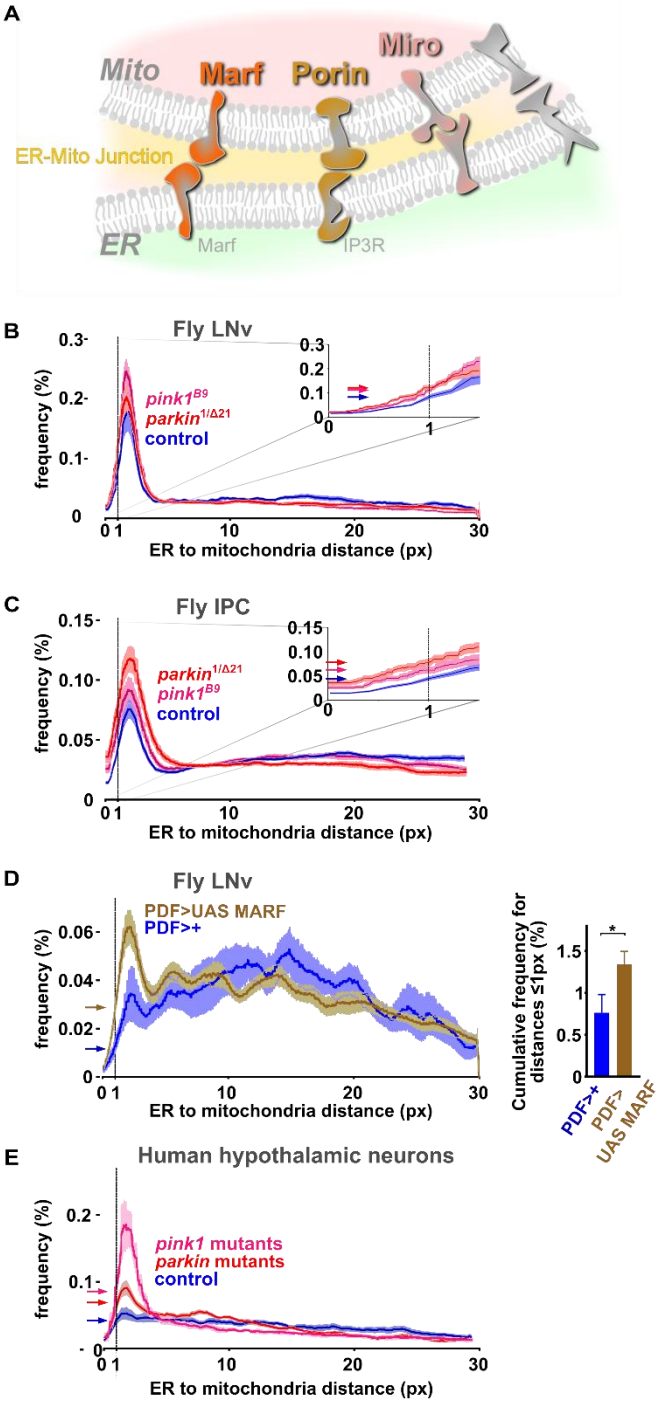

Figure S6. ER-mitochondrial contacts in *pink1* and *parkin* mutants and animals that overexpress MARF. Related to Figure 6.

(A) Schematic of different protein complexes that span the ER-mitochondrial membranes and promote ER-mitochondrial junction formation.

(B-C) Distance histogram of the separation of ER and mitochondria in LNv neuron cell bodies (**B**) and IPC cell bodies (**C**) of control, *parkin* and *pink1* mutants. KDEL-GFP (ER) labeling and mito-tdtomato labeling (PDF-Gal4) were thresholded and for each pixel on the surface of the ER labeling the distance to the closest mitochondrial pixel was calculated. The data in panel B and C relate to the images and quantification in Figure 6A-B and Figure 6C-D respectively. n=7-9 brains for B and 16-24 brains for C per condition.

(D) Distance histogram (left, calculated as in B-C) of the separation of ER and mitochondria in LNv neuron cell bodies and quantification of the extent of the contacts between ER and mitochondria (right, ie. quantification of the frequency of ER pixels within a distance of one pixel from mitochondria upon overexpression of MARF in LNv (PDF-Gal4). n=6-12 brains per condition. **p*<0.05 by Mann-Whitney test. Data are represented as mean ± SEM.

(E) Distance histogram of the separation of ER and mitochondria of controls, *parkin* and *pink1* mutant patients. anti-PDI (ER) labeling and anti-TOM-20 labeling in VIP positive neurons were thresholded and for each pixel on the surface of the ER labeling, the distance to the closest mitochondrial pixel was calculated. The data in panel E relates to the images and quantification in Figure 6F-G. n=16-20 neurons per genotype from two independent differentiations.

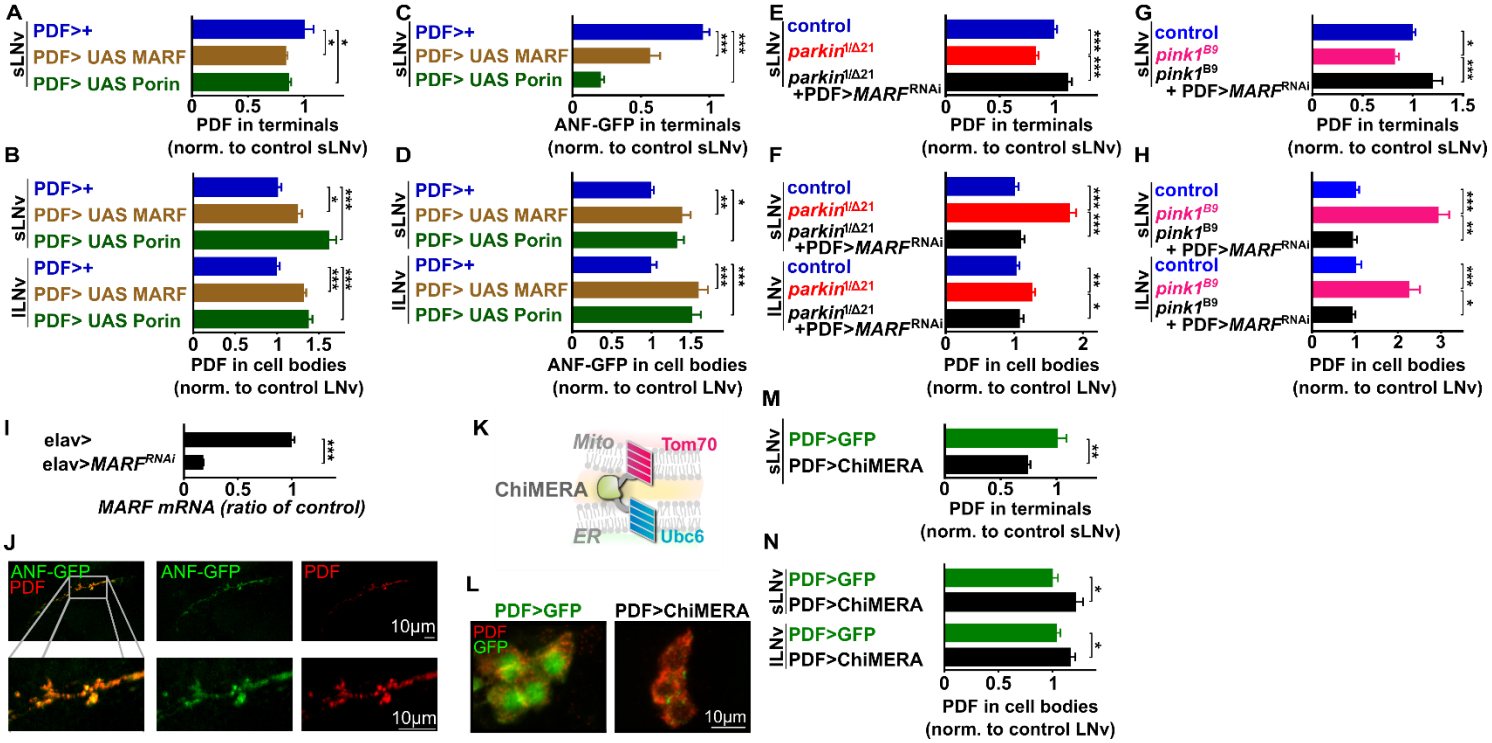

Figure S7. ER-mitochondrial contacts control neuropeptide distribution. Related to Figure 7.

(A-D) Quantification of anti-PDF labeling intensity (A-B) or ANF-GFP fluorescence intensity (C-D) in LNv terminals (A, C) or LNv cell bodies (B, D) of animals overexpressing Porin or MARF in LNv neurons (PDF-Gal4, A,B) and in animals also expressing ANF-GFP in LNv neurons (C and D). Animals were dissected at *Zeitgeber* time 23 and images are shown in Figure 7B-C. n=31-58 animals in A-B and n=14-16 animals in C-D. *p<0.05, **p<0.01, ***p<0.001 by Bonferroni's test following one-way ANOVA. Data are represented as mean ± SEM.

(E-H) Quantification of anti-PDF labeling intensity in LNv terminals (E, G) or LNv cell bodies (F, H) of *parkin* (E, F) and *pink1* (G, H) mutants that do or do not express $MARF^{RNAi}$ in LNv neurons (PDF-Gal4). Animals were dissected at *Zeitgeber* time 23 and images are shown in Figure 7E-F. n=35-59 animals in E-F and n=7-61 animals in G-H. *p<0.05, **p<0.01, ***p<0.001 by Bonferroni's test following one-way ANOVA. Data are represented as mean ± SEM.

(I) Quantitative RT-PCR of *MARF* RNA in brains that express RNAi to *MARF* under control of Elav-Gal4 (VDRC 105261). n=3 independent assays. ***p<0.001 by Mann-Whitney test. Data are represented as mean ± SEM.

(J) Imaging of LNv neuron terminals that express ANF-GFP (a DCV marker) labeled with anti-PDF indicating extensive co-localization also at the level of single vesicles resident at terminals.

(K) ChiMERA bridges the mitochondrial and ER membrane to induce additional contacts between these organelles.

(L) Images of ChiMERA fluorescence and of cytoplasmic GFP fluorescence each expressed in LNv neurons (PDF-Gal4), indicating diffuse labeling of GFP and restricted labeling of ChiMERA – characteristic of ER-mitochondrial junctions.

(M-N) Quantification of anti-PDF labeling intensity in LNv terminals (M) or LNv cell bodies (N) of animals that express ChiMERA in LNv neurons (PDF-Gal4). Animals were dissected at *Zeitgeber* time 23 and images are shown in Figure 7I. n=38-56 animals. **p<0.01 by Mann-Whitney test in M and *p<0.05 by Bonferroni's test following one-way ANOVA in N. Data are represented as mean ± SEM.

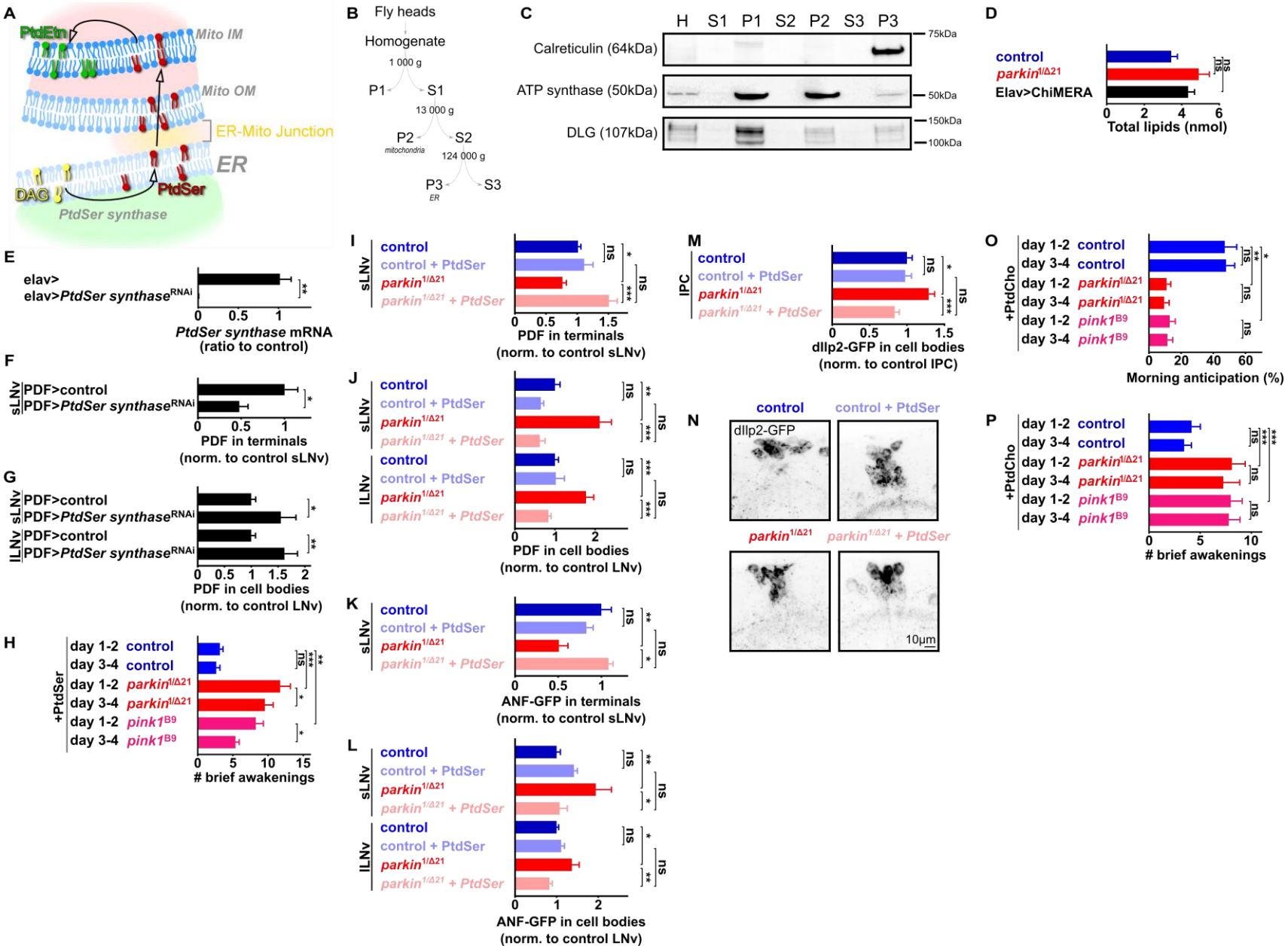
A
PtdEtn
Mito IM
Mito OM
ER-Mito Junction
ER
DAG
PtdSer
PtdSer synthase
B
Fly heads
Homogenate
1 000 g
P1
S1
13 000 g
P2
mitochondria
S2
124 000 g
P3
ER
S3
C
H S1 P1 S2 P2 S3 P3
Calreticulin (64kDa)
ATP synthase (50kDa)
DLG (107kDa)
75kDa
50kDa
150kDa
100kDa
D
control
parkin1/Δ21
Elav>ChiMERA
Total lipids (nmol)
E
elav>
elav>PtdSer synthaseRNAi
PtdSer synthase mRNA
(ratio to control)
F
sLNv
PDF>control
PDF>PtdSer synthaseRNAi
PDF in terminals
(norm. to control sLNv)
G
sLNv
lLNv
PDF>control
PDF>PtdSer synthaseRNAi
PDF in cell bodies
(norm. to control LNv)
H
+PtdSer
day 1-2 control
day 3-4 control
day 1-2 parkin1/Δ21
day 3-4 parkin1/Δ21
day 1-2 pink1B9
day 3-4 pink1B9
brief awakenings
I
sLNv
control
control + PtdSer
parkin1/Δ21
parkin1/Δ21 + PtdSer
PDF in terminals
(norm. to control sLNv)
J
sLNv
lLNv
PDF in cell bodies
(norm. to control LNv)
K
ANF-GFP in terminals
(norm. to control sLNv)
L
ANF-GFP in cell bodies
(norm. to control LNv)
M
lPC
dllp2-GFP in cell bodies
(norm. to control lPC)
N
control
control + PtdSer
dllp2-GFP
parkin1/Δ21
parkin1/Δ21 + PtdSer
10µm
O
+PtdCho
day 1-2 control
day 3-4 control
day 1-2 parkin1/Δ21
day 3-4 parkin1/Δ21
day 1-2 pink1B9
day 3-4 pink1B9
Morning anticipation (%)
P
+PtdCho
brief awakenings

Figure S8. PtdSer rescues circadian and sleep pattern defects of *parkin* and *pink1* mutants. Related to Figure 8.

(A) Schematic of lipid distribution between ER and mitochondria. Lipid synthesis occurs in the ER: Diacylglycerol (DAG) is metabolized to Phosphatidylserine (PtdSer) by PtdSer synthase at the ER-mitochondria contacts. PtdSer is then transported to mitochondria in an ER-mitochondria junction dependent manner. In mitochondria, PtdSer decarboxylase subsequently degrades PtdSer to Phosphatidylethanolamine (PtdEtn).

(B) Overview of the differential centrifugation protocol used to isolate ER/golgi and mitochondria-enriched fractions and indication of the fractions used in (C).

(C) Western blot of the different fractions obtained by differential centrifugation of control heads to indicate the enrichment of organelles in each fraction (data for the other genotypes shown in (D) are very similar and not shown). Equal amounts of protein were loaded in each lane. The ER marker Calreticulin is mostly present in the fraction P3; the mitochondrial marker ATP Synthase is enriched in fraction P2; note there is little contamination of the post-synaptic compartment (anti-DLG) in the fractions P2 and P3. Fractions P2 and P3 of control, *parkin* mutant and ChiMERA (Elav-Gal4) expressing fly heads were used for lipidomics.

(D) Mass spectrometry and quantification of the total amount of lipids in the homogenates of control, *parkin* mutant and ChiMERA-expressing flies. n=3-5 independent mass spectrometry runs. ns: not significant by Bonferroni's test following one-way ANOVA. Data are represented as mean ± SEM.

(E) Quantitative RT-PCR of *PtdSer synthase* RNA in fly heads that express RNAi to *PtdSer synthase* under control of Elav-Gal4 (VDRC 105470). n=3 independent assays. **p<0.01 by Mann-Whitney test. Data are represented as mean ± SEM.

(F-G) Quantification of anti-PDF labeling intensity in LNv terminals (F) or LNv cell bodies (G) of animals that express *PtdSer synthase*^{RNAi} in LNv neurons (PDF-Gal4). Animals were dissected at *Zeitgeber* time 23 and images are shown in Figure 8B. n=9-15 flies. *p<0.05, **p<0.01 by Bonferroni's test following one-way ANOVA in F and *p<0.05 by Mann-Whitney test in G. Data are represented as mean ± SEM.

(H) Quantification of brief awakenings (24 h) upon feeding control, *parkin* and *pink1* mutant flies 150 µM (final concentration in the food) PtdSer. Data for the first two days of feeding (day 1-2) were pooled and data for the consecutive two days of feeding (day 3-4) were pooled. Note that after 3-4 days of feeding the brief awakenings defect is partially rescued, as is the defect in morning anticipation (shown in Figure 8D). Longer periods of feeding do not yield stronger rescue of the brief awakenings phenotype (not shown). n=4 assays with 25 flies each. ns: not significant; *p<0.05, **p<0.01, ***p<0.001 by Tukey's test following two-way ANOVA. Data are represented as mean ± SEM.

(I-L) Quantification of anti-PDF labeling intensity (I-J) or ANF-GFP fluorescence intensity (K-L) in LNv cell bodies (I, K) or LNv terminals (J, L) upon feeding control *parkin* and *pink1* mutant flies for 4 days 150 µM (final concentration in the food) PtdSer. Animals were dissected at *Zeitgeber* time 23 and images are shown in Figure 8E-F. n=5-16 animals in I-J and n=4-18 animals in K-L. ns: not significant; *p<0.05, **p<0.01, ***p<0.001 by Tukey's test following two-way ANOVA. Data are represented as mean ± SEM.

(M-N) Quantification of fluorescence intensity in cell bodies (M) and images (N) of dIlp2-GFP expressed in IPC neurons (Ilp2-Gal4) upon feeding control and *parkin* mutant flies for 4 days 150 µM (final concentration in the food) PtdSer. Animals were dissected at *Zeitgeber* time 23. n=8-10 animals. ns: not significant, *p<0.05, ***p<0.001, by Tukey's test following two-way ANOVA. Data are represented as mean ± SEM.

(O-P) Quantification of morning anticipation (O) and brief awakenings (24 h) (P) upon feeding control, *parkin* and *pink1* mutant flies 300 µM (final concentration in the food) PtdCho. Data for the first two days of feeding (day 1-2) were pooled and data for the consecutive two days of feeding (day 3-4) were pooled. Note that PtdCho does not rescue the phenotypes in the mutants. We also tested lower concentrations of PtdCho (30 µM) and PtdSer (15 µM) and both these also do not rescue the behavioral defects in *pink1* and *parkin* mutants (not shown). Longer periods of feeding also do not yield rescue (not shown). n=3-6 assays with 25 flies each. ns: not significant, *p<0.05, **p<0.01 by Tukey's test following two-way ANOVA. Data are represented as mean ± SEM.